multi-**Risk** **sciEnce** for **resilienT** **commUnities** **undeR** a **changiNg** climate

Codice progetto MUR: **PE00000005** – CUP LEADER PARTNER C93C22005160002

Deliverable title: Near shore and coastal areas, volcanic islands: thematic maps inducing hazard severity indicators and zoning for coupled/combined triggers

Deliverable ID: 2.4.2

Due date: May 30th 2025

Submission date: May 29th 2025

AUTHORS

Silvia Ceramicola (OGS); Matteo Berti (UniBo); Marco Bianchini (OGS, Sapienza); Marco Bracci (UniPa); Valeria Lo Presti (UniPa); Giovanni Poneti (OGS), Elena Scacchia (Ispra); Nicolo Parrino (UniPa); Filippo Zaniboni (UniBo)

1. Technical references

Project Acronym	RETURN
Project Title	multi-Risk sciEnce for resilienT commUnities undeR a changiNg climate
Project Coordinator	Domenico Calcaterra UNIVERSITÀ DEGLI STUDI DI NAPOLI FEDERICO II domcalca@unina.it
Project Duration	December 2022 – November 2025 (36 months)

Deliverable No.	DV 2.4.2
Dissemination level*	PU
Work Package	WP4 - Trigger-based multiple geohazard scenarios
Task	T 2.4.1 -
Lead beneficiary	OGS
Contributing beneficiary/ies	Ispra, UniBo , UniPA

* PU = Public

PP = Restricted to other programme participants (including the Commission Services)

RE = Restricted to a group specified by the consortium (including the Commission Services)

CO = Confidential, only for members of the consortium (including the Commission Services)

Document history

Version	Date	Lead contributor	Description
0.1	30.04.2025	S, Ceramicola (OGS); M. Berti (UniBo); M. Bianchini (OGS. Sapienza); M. Bracci (UniPa); V. Lo Presti (UniPa); G. Poneti (OGS), E. Scacchia (Ispra); N. Parrino (UniPA), F. Zaniboni (UniBo)	Final draft for Spoke review
0.2	14.05.2025	S, Ceramicola (OGS); M. Berti (UniBo); M. Bianchini (OGS. Sapienza); M. Bracci (UniPa); V. Lo Presti (UniPa); G. Poneti (OGS); E. Scacchia (Ispra); N. Parrino (UniPA), F. Zaniboni (UniBo)	Critical review and edits for approval
1.0	31.05.2025	S, Ceramicola (OGS); M. Berti (UniBo); M. Bianchini (OGS. Sapienza); M. Bracci (UniPa); V. Lo Presti (UniPa); G. Poneti (OGS); E. Scacchia (Ispra); N. Parrino (UniPA), F. Zaniboni (UniBo)	Final version

2. Abstract

Geohazards assessment in marine environments is challenging due to the dynamic nature of the seabed, the complexity of underwater environments, and the difficulty of direct observation. This necessitates the use of advanced technologies and methodologies to assess geohazards like submarine landslides and tsunamis, which pose significant threats to Europe's increasingly populated coastlines and infrastructures. The Mediterranean is one of the most geodynamically active regions in the world, making it even more crucial to develop effective risk mitigation strategies. In this peculiar tectonically active setting, the proximity of coasts and narrow continental shelves enables landslides occurring along canyon heads or open slopes to generate tsunamis that reach shorelines within minutes, often rendering ineffective early warning systems. These strategies are necessary not only for coastal areas, where vulnerable communities and infrastructure are located but also for deep-water infrastructures, especially to facilitate the ongoing energy transition and safeguard vulnerable assets from marine geohazards.

In the last decade, the rapid advancement of marine technologies has enabled the marine geological community to identify and characterize marine geohazards at increasingly higher resolution along the continental margins of many countries. In Italy, the MAGIC project, through extensive high-resolution bathymetric campaigns (up to 10m of geometric resolution), provided a detailed morphological characterization of major marine geohazards along the Italian coasts, offering valuable case studies to deepen our understanding of the driving mechanisms and functioning of related geological processes. We used these case studies as Learning Examples (LEs) in the RETURN project to analyse and, for the first time, to quantify the predisposing, preparatory factors, and triggers, responsible for ground instabilities and their coastal impacts. We have focused on the occurrence of submarine landslides with rapid kinematics, as they are able to quickly displace large volumes of water column, possibly generating tsunamis within a short time. Unfortunately, the limited number of representative examples has significantly constrained similar analyses for other types of submarine ground instabilities, such as landslides with slow kinematics, liquefaction-related failures, and landslides occurring on steep submarine cliffs

RETURN Task 2.4.1 (Multiple Geohazards for Ground Instabilities in Near-Shore and Coastal Areas, Volcanic Islands) focused on the two main recurrent geological environments relevant for ground instabilities: open slopes and canyon headwalls. Both settings can host submarine landslides, though varying in size, volume, and recurrence, and have the potential to trigger tsunamis with detrimental impacts on coastal communities and infrastructures.

As part of RETURN Milestone 5, we developed new methodological advancements in the quantification of submarine rapid landslides assessment, aimed at improving nearshore and coastal risk mitigation strategies. The main challenges and constraints are explained in this Deliverable, where we describe, for the first time, the following key results achieved:

- Validation of a toolchain workflow for the marine environment for rapid landslide assessment.
- Generation the first submarine landslide susceptibility maps for Italy (Calabria and Sicily) to analyse the influence of key landslide predisposing factors.
- Development of several reliable analytical tools able to quantify preparatory factors and triggers responsible of initiating rapid ground instabilities and their coastal impacts.
- Development of an analytical tool to calculate the coastal flooding on the base of the tsunamis intensity.

The new validated toolchain workflow for rapid marine landslides will be used to model hazard scenarios within the RETURN Virtual Test Bed (VTB), a digital platform builds in within TASK 2.4.1 using high-resolution digital elevation model (up to 5 cm) derived from LE's for testing, modelling, and analysing real-world processes. Insights from VTB scenarios will support the development of a Proof of Concept (PoC) for rapid submarine landslides at both local, canyon heads and regional open slope scales.

3. Table of contents

Summary

List of Figures

List of tables

4. 4. First Chapter: Introduction

Geohazard assessment in the marine environment is inherently challenging due to the unique characteristics of underwater landscapes. The dynamic nature of the seafloor, influenced by factors such as tectonic activity, sediment transport, fluid migration, and varying oceanographic conditions, presents challenges in hazard prediction. Additionally, the difficulty of accessing deep-sea environments for direct observation and data collection further complicates the assessment process. Therefore, marine geohazard assessments must rely on advanced technologies like remote sensing, seismic imaging, and sediment coring, combined with methods that integrate environmental, geological, and hydrodynamic factors, to accurately assess the likelihood of hazards such as submarine landslides, tsunamis, and underwater volcanic activity.

Submarine landslides are mass movements of sediment, rocks, and debris down the seafloor, usually along continental slopes, canyon heads and walls, or volcanic flanks. Submarine landslides can be significantly larger than any terrestrial landslide and have the potential to generate tsunamis with far-reaching effects comparable to those caused by earthquake-generated tsunamis. Even small landslides can affect expensive and critically important seafloor or coastal assets, especially when they occur in proximity or exhibit retrogressive character. The two primary offshore geological settings associated with ground instabilities are open slopes and canyon headwalls (Fig. 1). Open slopes can generate larger landslides with longer recurrence time, sometimes never failing again. In contrast, landslides in canyon headwalls are typically smaller in size, more frequent, and responsible for the retrogressive erosion of certain canyon systems toward the coast. Both settings can trigger submarine landslides with the potential to generate tsunamis, significantly impacting coastal communities and infrastructure.

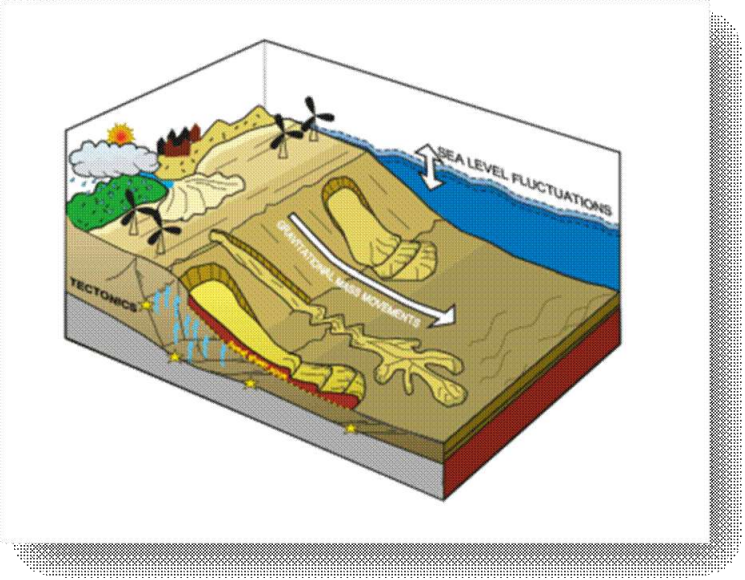

Figure 1 Sketch of a continental slope incised by ground instabilities in the open slope (on the sides) and in canyon headwalls (in the middle).

Landslides can have rapid or slow kinematics. Rapid kinematics means that the landslide's movement is fast, potentially covering kilometres of distance in a short time (minutes to hours). Fast-moving submarine landslides can displace large volumes of the water column suddenly and thus can generate tsunamis. Tsunamis may cause major damage to coastal communities and/ or to seafloor infrastructure like communication cables and oil pipelines, or redistribute sediments quickly, impacting marine ecosystems. In contrast, some submarine landslides are slow-moving, creeping along the seabed over years or decades without triggering immediate

hazards — but those with rapid kinematics are sudden and dangerous. In the Mediterranean Sea, due to the proximity of the coasts and the typically narrow continental shelves, landslides occurring along canyon heads or on the slopes can produce tsunamis that reach shorelines within minutes, making early warning systems sometimes ineffective. To effectively mitigate the risks associated with the occurrence of submarine landslides and the resulting tsunamis, it is essential to implement extensive monitoring of seabed areas identified as critical, while simultaneously advancing a detailed geological and geotechnical understanding of the factors controlling slope instability, to better anticipate where and under what conditions future landslides are most likely to initiate. Despite its crucial role in understanding marine geohazards, only a limited number of studies have focused on the characterization of submarine landslide susceptibility (Nian et al., 2019; Innocenti et al. 2020; Avdievitch and Coe, 2022). Susceptibility analysis is the first essential step for an effective assessment, as it allows for the examination and interrelation of preconditioning factors to evaluate the likelihood of a landslide occurring. The second critical step involves analysing the preparatory factors within a specific area, which further influence and intensify the preconditioning conditions, thus refining the overall risk assessment and providing a more accurate prediction of landslide potential. This can be achieved by studying Learning Examples (LES) (Fig. 2), such as areas of the seabed affected by fluid escapes or by weak sediment layers, and by identifying the parameters responsible for sediment instabilities. This allows for better control of the factors contributing to landslide risk.

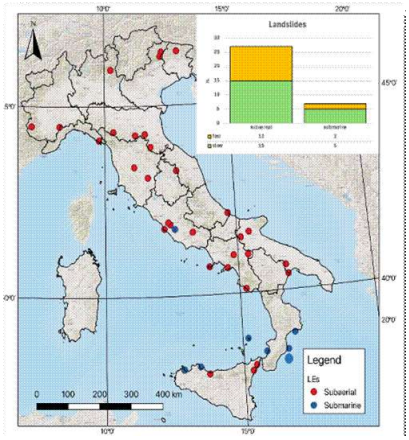

Figure 2 Learning Examples (LEs) of Italian seascapes (in blue), identified during the MAGIC project, which helped to constrain various geological processes that reduce slope stability.

Building on the characterization of marine geohazards achieved during the MAGIC project (Fig. 3), RETURN Milestone 5, Task 2.4.1, marked a significant advancement by transitioning from qualitative descriptions (seabed mapping) to the quantitative assessment of submarine landslides characterized by rapid kinematics. The geological insights gained from Learning Examples (LEs) from Italian seascapes, which helped to constrain various geological processes that reduce slope stability, enabled further progress, resulting in new significant methodological advancements aimed at improving nearshore and coastal geohazard risk mitigation. This was achieved through the development of the first susceptibility maps of southern Italy and the quantification, for the first time, of preconditioning factors, preparatory processes, and triggers ultimately enhancing our ability to assess the likelihood of submarine landslides and their potential impacts on coastal environments.

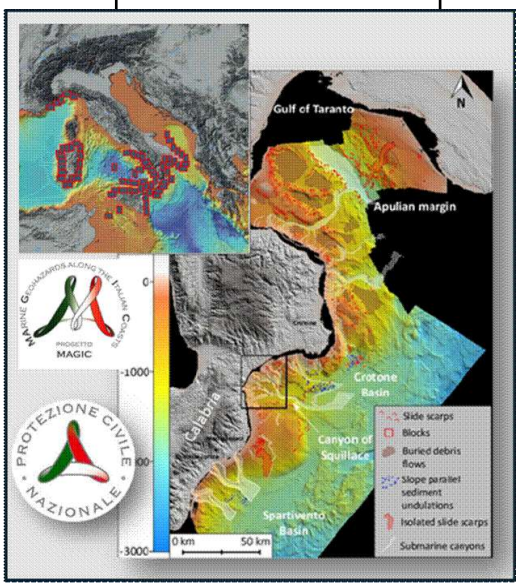

Figure 3 First maps of the marine geohazards along the Calabrian and Apulian margins (Ceramicola et al 2014). The inset shows the 72 sheets produced during the Magic Project, where the morphologies of major marine geohazards were mapped across the Italian Seas.

4.1 Preconditioning Preparatory and Triggers and multihazard

In marine environments, understanding the interplay between preconditioning, preparatory factors, and triggers is critical for assessing and managing multihazard risks. These environments are dynamic and complex, influenced by a range of natural and anthropogenic processes that can interact to create cascading or compound hazards.

Preconditioning refers to the long-term environmental states or processes that make an area more susceptible to hazards. In the marine context, this could include gradual processes like sediment accumulation on the continental slope, coral reef degradation, or long-term sea level rise. These conditions don't cause immediate failure or disaster but set the stage for heightened vulnerability. For instance, sediment overloading on underwater slopes can weaken structural stability over time, creating a situation where even a relatively minor event could trigger a major submarine landslide.

Preparatory factors are changes that further modify the preconditioned environment, bringing it closer to a tipping point. Examples in marine settings include intense periods of sediment deposition from river outflows, bioturbation from marine organisms, or tectonic stresses accumulating along fault lines under the seafloor. These processes continue to weaken or destabilize the environment, making it increasingly sensitive to external forces.

Triggers are the immediate causes of a hazard event. In marine environments, triggers could include earthquakes, large storm waves, sudden shifts in ocean currents, or even human activities like offshore drilling or deep-sea mining. A relatively minor earthquake might not cause a landslide in a stable marine slope, but in one that has been preconditioned and further weakened by preparatory processes, it could result in massive underwater slides, generating tsunamis or damaging underwater infrastructure.

In marine environments, the concept of **multiple hazards** refers to the coexistence of different hazardous processes—such as submarine landslides, earthquakes, and tsunamis—that can impact the same area, either independently or simultaneously, significantly increasing the overall level of risk. Beyond this, **cascading**

hazards represent a critical dynamic, where the occurrence of one event initiates a chain reaction, triggering additional processes that amplify the consequences. For instance, a submarine landslide can rapidly displace large volumes of water, generating a tsunami that impacts coastal communities and critical infrastructures. Understanding the interplay between multiple and cascading hazards is therefore essential for developing integrated risk mitigation strategies, particularly in complex and highly dynamic settings like the Mediterranean region.

Understanding the complex web of preconditioning, preparatory factors, triggers, and multihazard interactions in marine environments is crucial for effective risk assessment and disaster preparedness. It requires an interdisciplinary approach, integrating geology, engineering geology, oceanography and the impact of a rapidly changing climate, to build resilient marine infrastructures and protect vulnerable ecosystems and coastal populations.

As part of RETURN Milestone 5, within Task 2.4.1, we advanced the assessment of submarine landslides by focusing on the quantification of preconditioning factors (through the development of the first susceptibility maps for Calabria and Sicily), preparatory processes, and triggers responsible for initiating rapid ground instabilities. These results, presented in the following chapters, represent a key step toward improving the understanding of landslide likelihood in the marine environments and their potential coastal impacts.

4.2 Susceptibility analyses in marine environment

In the Mediterranean Sea, the limited width of continental shelves and the proximity between slopes and coastal areas result in tsunamis generated by submarine landslides reaching the shore within very short timeframes, often compromising the effectiveness of early warning systems. To address this challenge, it is crucial to enhance our knowledge of the seafloor, extensively monitor areas identified as particularly critical, and develop high-resolution susceptibility maps that identify zones most prone to failure, enabling a more targeted and effective approach to risk mitigation.

Hazard is an event posing a threat to life, health, property or environment. Hazard assessment is the evaluation of the occurrence of a potentially damaging event, (where, when, how frequently, magnitude). The identification of hazards is the first step in performing hazard assessment. Risk is the probability that a specific hazard will cause harm. Thus, a hazard poses no risk if there is not vulnerability to that hazard

Susceptibility analyses in marine environments aim to evaluate the likelihood of seafloor areas to specific hazards, such as submarine landslides, sediment remobilization, fault reactivation, or gas seepage. Risk assessment in the context of geohazards, such as submarine landslides, is closely related to susceptibility because susceptibility forms the foundation of understanding the likelihood of a hazardous event occurring. In this context, susceptibility refers to the inherent characteristics of a region that make it more prone to certain types of hazards, such as landslides or tsunamis. In the marine environment these analyses are crucial tools for understanding and predicting areas prone to specific geohazards, such as submarine landslides, sediment remobilization, or fault reactivation. Unlike deterministic approaches, susceptibility assessments focus on identifying *where* hazardous events are more likely to occur, without necessarily predicting *when* they will happen. This method provides a foundational layer for multi-hazard risk evaluations, marine spatial planning, and the design of offshore infrastructure.

In practice, susceptibility mapping involves integrating multiple datasets: seabed morphology derived from bathymetry, sub-seafloor structures revealed by seismic profiles, sediment characteristics from cores, and, increasingly, time-lapse data from emerging technologies like Distributed Acoustic Sensing (DAS). Each parameter acts like a clue in a complex puzzle. For example, areas of steep slope angles, the presence of weak sediment layers (such as clay-rich deposits), and proximity to active faults often correlate strongly with elevated susceptibility to slope failure.

A typical analysis may use statistical models or machine learning algorithms to weigh these factors. For instance, a random forest model might learn from known landslide locations to predict high-risk zones elsewhere on the seabed. Alternatively, simpler heuristic methods can assign susceptibility scores based on expert judgment, which remains a valuable approach when data is limited or heterogeneous.

Susceptibility assessments are crucial to gain a comprehensive view of their distribution and the potential damage they may cause to infrastructure planning (pipelines, cables, offshore platforms) (Harbitz et al. 2014) and for evaluating potential cascading effects, such as tsunami generation from submarine landslides (Løvholt et al. 2025). They also serve as the foundation for multi-hazard assessments, especially in tectonically active or rapidly sedimenting margins. Unlike in terrestrial settings where landscapes may remain stable for centuries, submarine environments can shift dramatically over just a few years, making regular updates to susceptibility models necessary.

Susceptibility maps do not guarantee an event but highlight "hazard-prone" zones under specific conditions. Their value lies both in guiding site investigations and monitoring efforts, but also in building resilient strategies for future marine operations.

Despite its critical importance for understanding marine geohazards, only a limited number of studies have addressed the characterization of submarine landslide susceptibility. Research by Nian et al. (2019) and Avdievitch and Coe (2022) explored susceptibility across different geological settings, while Innocenti et al. (2020) extended the analysis to a regional scale. However, these studies present several limitations. Many assessments rely on relatively coarse spatial resolutions, sometimes simplifying too much the complex variability of seafloor properties. In addition, susceptibility models often focus predominantly on geomorphological or slope-related parameters, without fully integrating geotechnical data, sedimentary processes, or dynamic triggering factors such as seismic loading. Regional-scale approaches, while valuable, may overlook important local variations that strongly influence landslide initiation. Overall, although these contributions represent important advances, further work is needed to develop more integrated, high-resolution, and multidisciplinary frameworks for evaluating submarine landslide susceptibility across different marine environments.

In RETURN Milestone 5, within WP4 task 2.4.1, thanks to tight collaboration with geologist's expert in terrestrial ground instabilities, we successfully applied tools and methodologies originally designed for onshore settings - where landslides are monitored at much higher resolution and with a greater number of measurable parameters- to the marine environment. This transfer of knowledge was made possible through the availability of an extensive landslide inventory along the southern Italian continental margins (more than 2000 events), compiled through the MAGIC project (Ceramicola et al, 2024 and 2025, Chiocci et al., 2011,). The findings are presented in the following chapters of this deliverable.

4.3 Submarine rapid landslides toolchain workflow in nearshore and open slopes

As part of RETURN Milestone 5, within Task 2.4.1, we advanced the assessment of submarine landslides by focusing on the quantification of preconditioning factors through the development of the first susceptibility maps for Calabria and Sicily. In addition, we developed five new reliable analytical tools that quantify preparatory processes, and triggers responsible for initiating rapid ground instabilities:

- **Susceptibility Mapping (Preconditioning)** – two methods
- **FOS (Factor of Safety) Modeling (Preparatory)**
- **Tsunami Propagation Analysis (Triggering)**
- **Flooding Impact Assessment (Triggering)**

These tools were integrated in the first toolchain workflow for submarine landslide assessment (Fig 4). The new workflow combines algorithms and numerical models that quantify:

- the susceptibility of landslides in open slopes and canyon heads
- the Factor of Safety for Active Fluid Seepages
- Tsunami wave propagation and flooding

This framework is innovative, as it links the driving mechanisms responsible for ground instabilities to their impact on coastal regions.

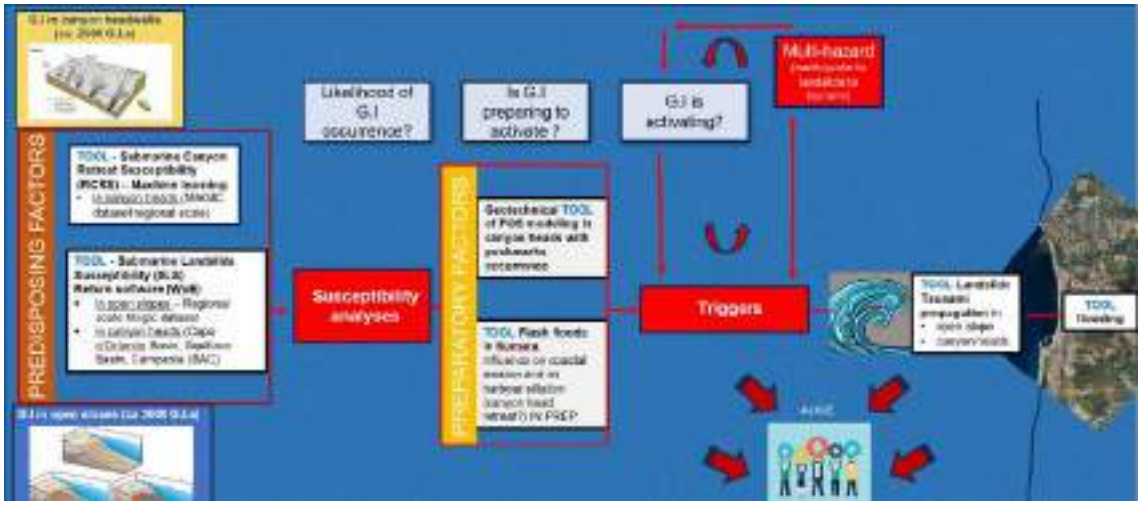

Figure 4 The new Toolchain workflow for rapid landslides in marine environment developed within RETURN Milestone 5, in Task 2.4.1.

These results represent a key step toward improving the understanding of landslide likelihood and their potential coastal impacts. The main challenges and constraints are outlined in the next chapters of this Deliverable 2.4.2 where we present, for the first time, the key results achieved as part of RETURN Milestone 5, Task 2.4.1. over the past six months.

5. 5. Second Chapter: Marine Toolchain Workflow

Input data is an essential element for the operation of the proposed working tools. Indeed, they allow their application into different geological and geomorphological contexts and to obtain results in terms of the possible occurrence of different ground instabilities. Given the significant difference in terms of the quantity of data available and their quality that currently persists between the terrestrial and marine contexts, such a distinction is maintained here by treating the uncertainty of the input data separately in the two contexts analysed in the project at which different environments belong to.

5.1 Canyon Retreat Susceptibility analyses using multivariate linear regression

The ability to assess and map areas susceptible to canyon head retreat is needed for effective coastal zone management and its geohazard mitigation. This tool provides a standardized methodology for quantifying submarine canyon retreat susceptibility along continental margins by implementing a multivariate regression model that integrates morphological and tectonic variables. The approach allows for comprehensive susceptibility assessment at regional scales, enabling prioritization of monitoring efforts and informing coastal planning decisions.

5.1.1 Method

The methodological foundation of this tool rests on the identification and georeferencing of submarine canyon heads through a process that combines bathymetric data interpretation with geospatial analysis. Using high-resolution multibeam bathymetric data from the Marine Geohazards along the Italian Coasts project (MaGIC, Chiocci and Ridente, 2011), a comprehensive record of submarine canyon head detachment niches was delineated. Each canyon head was represented by a unique point termed a PICS (Figure 5, *Punto Identificativo del Canyon Sottomarino*), corresponding to the highest point of each mapped headscarps. This approach resulted in the identification of 2765 PICS along the Italian continental margins.

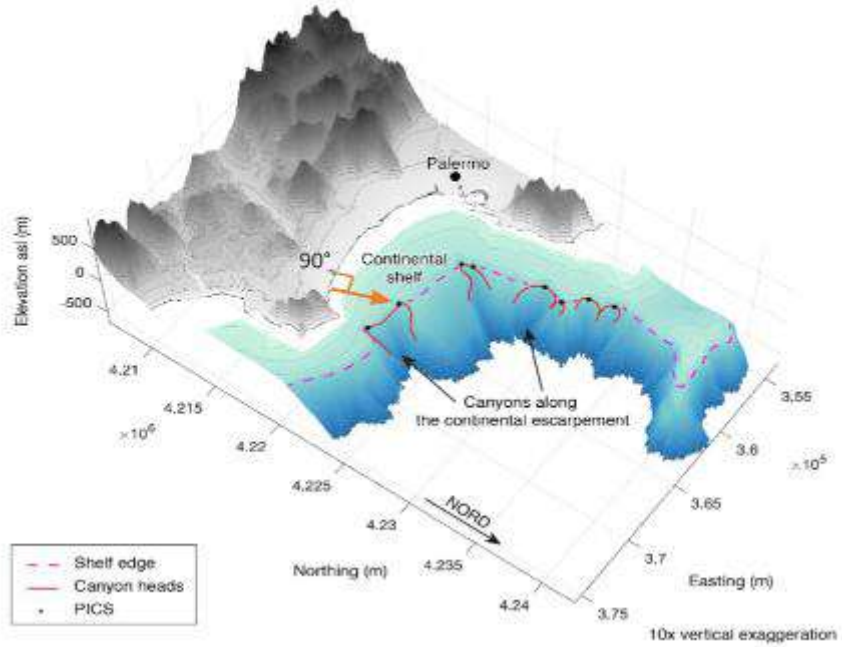

Figure 5 3D visualization of submarine canyons in the Gulf of Palermo (Italy) using LiDAR and multibeam data. Pink dashed line shows the shelf edge, red lines mark canyon heads, and black dots indicate PICS locations.

For each PICS, as shown in Figure 6, the proximity to the coastline was measured, serving as the dependent variable in the subsequent regression analysis (D'Ascola et al., 2022).

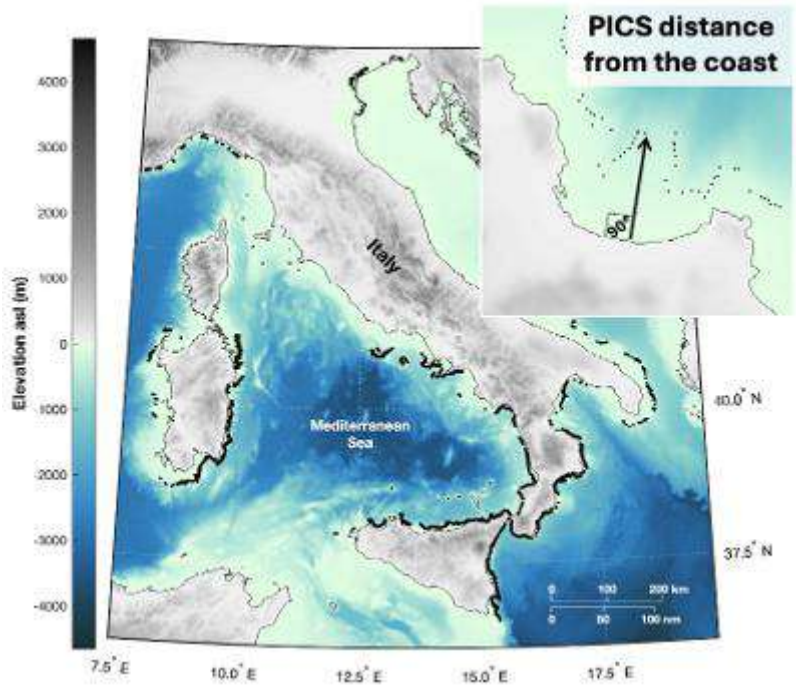

Figure 6 Black dots represent PICS location. In the upper-right panel an example of how the shortest distance between each individual PICS and the coastline was measured is shown.

This distance metric functions as a proxy for canyon head retreat susceptibility, where shorter distances indicate higher potential for retrogressive erosion processes that could impact coastal areas. The susceptibility assessment incorporated twelve independent variables categorized into morphological and tectonic factors:
Morphological Variables:

- Slope value at PICS location
- Distance between PICS and the nearest river mouth (Geoportale RNDT)
- Ratio between PICS-coast and PICS-river mouth distances
- Relief metric
- River mouth count within a 10 km radius from PICS

Tectonic Variables:

6. Uplift rate computed from literature of MIS 5.5 paleoshorelines (Ferranti et al., 2006)
7. Averaged coastal vertical deformation from Sentinel-1 InSAR data (Crosetto et al., 2021)
8. GNSS-derived vertical velocity field (Palano et al., 2017)
9. GNSS-derived horizontal velocity field (Palano et al., 2017)
10. Second invariance of horizontal strain rate (Palano et al., 2017)
11. Earthquake density from macroseismic-instrumental dataset (Rovida et al., 2020)
12. Earthquake density from synthetic epicentres (Rovida et al., 2020)

All variables underwent a data preprocessing workflow that included handling missing values through linear interpolation, standardization using Z-score, and linearization through appropriate transformations (logarithmic, square root, quadratic, etc.) based on statistical evaluation of fit metrics. The core of the tool employs a stepwise regression approach with bidirectional elimination to identify the most significant predictors of canyon retreat susceptibility evaluating the contribution of each regressor. The stepwise regression model, characterized by high explanatory power with an R-squared value exceeding 0.97, incorporates both individual predictors and the interaction terms between variables.
The susceptibility index (Si) for each location is calculated using the following equation:

$$S_i = \sum_{j=1}^{p} \beta_j X_{ij} + \sum_{k=1}^{q} \beta_k (X_{im} \times X_{in}) \quad \text{Eq. 1}$$

where:

- p is the number of individual predictors.
- q is the number of interactions terms.
- X_{im} and are the interacting variables.
- B_k is the coefficient for the interaction term.

The resulting susceptibility values are then classified into ten categories using quantile-based thresholds, providing a relative assessment of submarine canyon retreat susceptibility from "Very Low" to "Critical".

5.1.2 Results

The core of the Canyon Retreat Susceptibility Analysis tool is a MATLAB function called *calculateSusceptibilityToCoastalProximity* that implements the stepwise regression model to calculate susceptibility values for any set of PICS points with the required attribute data.

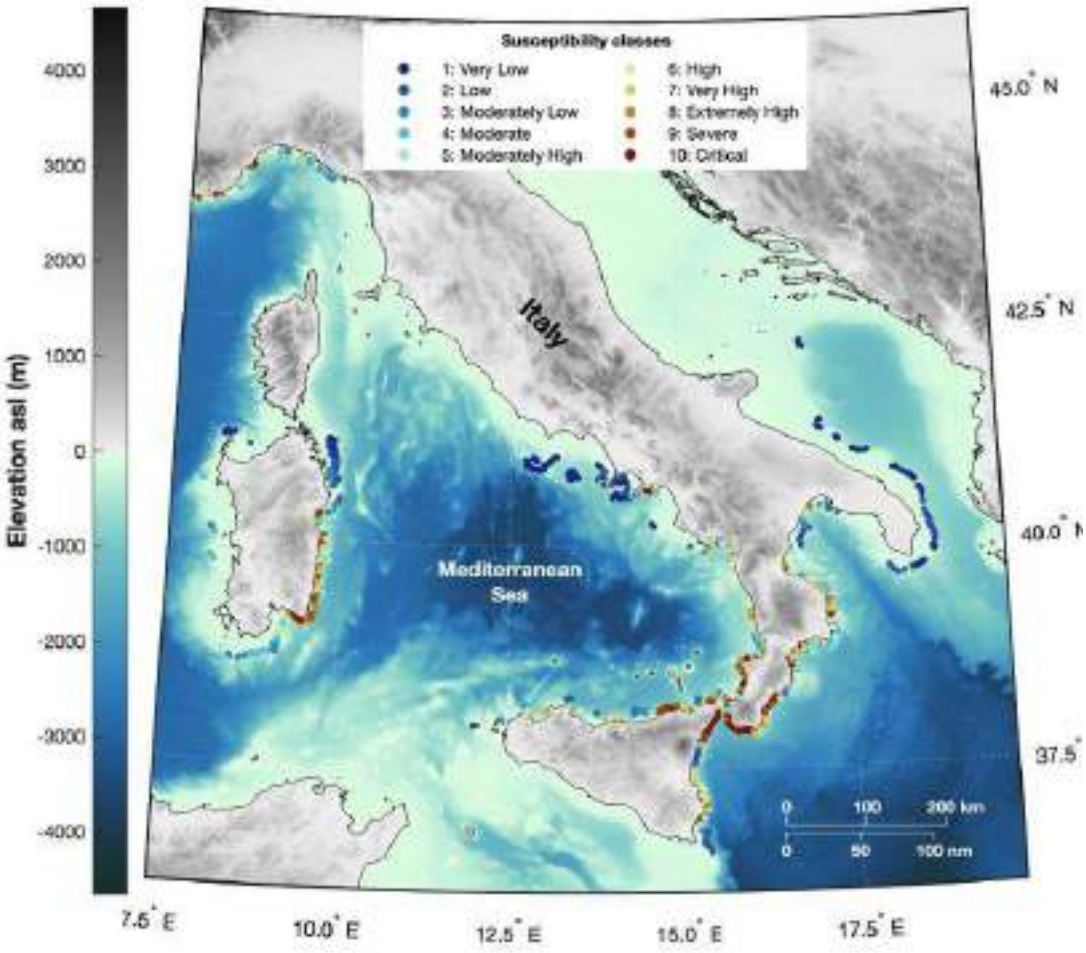

Figure 7 Susceptibility to submarine canyon retreat along the Italian margins. The colors range from very low (blue) to critical (red). Circles show PICS locations with their respective susceptibility values.

The tool accepts a dataset containing PICS locations and their associated morphological and tectonic attributes as input. It then performs the following operations:

1. Maps variable names between the regression model and the input dataset
2. Applies the precomputed regression coefficients to each variable and interaction term
3. Calculates the total susceptibility value for each PICS by summing all variable contributions
4. Classifies the susceptibility values into ten categories based on quantile distribution
5. Outputs the original dataset augmented with:
    - Numerical susceptibility values
    - Susceptibility class (1-10)
    - Text labels for each susceptibility class

The susceptibility calculation uses 55 precomputed coefficients derived from the regression analysis of 2765 Italian PICS and allows for a prompt susceptibility assessment without requiring model retraining. The tool's primary output is a classified susceptibility map that identifies areas of varying susceptibility to canyon head retreat (Figure 7). The tool provides flexibility in application, allowing users to:

- Apply the model to existing PICS datasets for rapid assessment
- Incorporate higher-resolution local data where available
- Recalculate susceptibility for new PICS locations using the precomputed model weights
- Perform targeted assessments in areas of special interest

5.1.3 Novelty, Criticalities and Relevance/Potentiality of this Tool

This tool represents the first comprehensive attempt to quantify submarine canyon retreat susceptibility at a national scale using a robust statistical framework establishing a methodological benchmark for similar assessments in other regions. The integration of morphological parameters with tectonic variables into a unified susceptibility model represents a significant advancement over previous approaches that typically considered these factors in isolation.

Despite the high explanatory power of the model ($R^2 > 0.97$), several limitations should be acknowledged. The static nature of the assessment does not account for temporal dynamics, including recurrence intervals and triggering thresholds. Future enhancements should incorporate time-series bathymetric data to capture evolution rates in high-susceptibility areas. Moreover, the quantile-based classification system provides a relative assessment rather than an absolute measure of hazard potential. While this approach is appropriate for prioritization and comparative analysis, it may not directly translate to absolute probability of failure or retreat rates. The developed tool offers significant potential for hazard management applications:

1. **Hazard Assessment and Mitigation:** By identifying areas with high susceptibility to canyon retreat, the tool provides valuable information for coastal zone management and infrastructure planning
2. **Prioritization of Monitoring Efforts:** Limited resources for marine monitoring can be directed toward the most susceptible areas identified by the tool.
3. **Methodological Framework:** The approach establishes a repeatable methodology that can be adapted to other regions.
4. **Integration with Cascading Hazard Models:** The susceptibility assessment provides a basis for modeling cascading hazards such as landslide-triggered tsunamis.

5.2. Susceptibility analysis using Weight of Evidence (WoE) method

Submarine landslides are gravity-driven sediment failures that occur along the seafloor, often affecting continental slopes, canyon systems, and sediment-rich basins. These events can pose serious risks to offshore infrastructure, trigger tsunamis, and shape the morphology of continental margins. Susceptibility assessment aims to identify areas prone to failure based on predisposing factors, without considering the timing or magnitude of events. In the submarine environment, this typically involves analyzing morphometric parameters (e.g., slope, curvature, roughness), geological context, and the spatial distribution of past landslides.
Despite challenges such as limited data availability and the complexity of submarine landslide processes, susceptibility models based on statistical or geotechnical approaches are poorly investigated even if these could be an essential tool for risk mitigation and marine spatial planning.

5.2.1 Method

The Weight of Evidence (WoE) method is a Bayesian probabilistic approach commonly used for landslide susceptibility modeling. It operates under the assumption of conditional independence between predictor variables and is particularly effective when working with categorical data or reclassified continuous variables. WoE evaluates the spatial correlation between the presence (D_1) and absence (D_0) of landslide events and various classes of conditioning factors (B_k) by computing the following weights:

$$W_k^{+} = ln\frac{P(B_k / D_0)}{P(B_k / D_1)}$$

$$W_k^{-} = ln\frac{1 - P(B_k / D_0)}{1 - P(B_k / D_1)}$$

Where:

- P(Bk|D1) is the conditional probability of landslides occurring in class Bk,
- P(Bk|D0) is the conditional probability of landslides not occurring in class Bk.

The contrast (C_k) for each class is then defined as:

$$C_k = W_k^{+} - W_k^{-}$$

The contrast values derived from the Weight of Evidence (WoE) method represent the statistical strength and direction of the relationship between each class within a predictor variable and the occurrence of submarine landslides. These classes—defined by the operator based on geomorphological thresholds and expert interpretation—allow for a detailed examination of how specific intervals of variables (such as slope, aspect, and curvature) are associated with landslide presence. High positive contrast values indicate a strong and statistically significant correlation with landslide occurrences, suggesting that those conditions favor instability. Conversely, negative contrast values imply conditions that are generally less susceptible to failure.

Each pixel in the study area is assigned a susceptibility score calculated as the sum of the weights (i.e., contrasts) of all predictor classes present at that location. This additive structure makes the WoE method

particularly suitable for spatial implementation within a GIS environment and facilitates sensitivity analyses and model interpretation. Importantly, the transparency of this approach allows for a clear understanding of the contribution of each environmental factor to overall landslide susceptibility.

To evaluate the performance of the susceptibility model, the Receiver Operating Characteristic (ROC) curve was used. This diagnostic tool plots the true positive rate (sensitivity) against the false positive rate (1 - specificity) for various threshold values, providing a graphical representation of model accuracy. The Area Under the Curve (AUC) summarizes the ROC curve into a single metric: values closer to 1.0 indicate excellent predictive capability, whereas values near 0.5 suggest no better performance than random guessing. In this study, the AUC values confirm that the WoE-based model effectively discriminates between areas prone to landslides and more stable regions of the seafloor.

Despite its advantages, the reliability of the WoE method depends on the independence of predictor variables. To reduce the risk of multicollinearity—where predictors are highly correlated and may distort weight estimates—preliminary statistical analyses such as Cramér's V coefficient or the Variance Inflation Factor (VIF) are commonly applied. These procedures help ensure that only the most relevant and independent variables are included in the final model, thereby enhancing its robustness and interpretability.

5.2.2 Regional scale application

Over 12,000 km² of high-resolution bathymetric data have been analyzed to identify, map, and characterize submarine landslides along the Ionian and Tyrrhenian continental margins, covering approximately 8,000 km² and 4,500 km² respectively (Fig. 8). This analysis led to the development of a comprehensive geodatabase comprising **1,945 submarine landslides**.

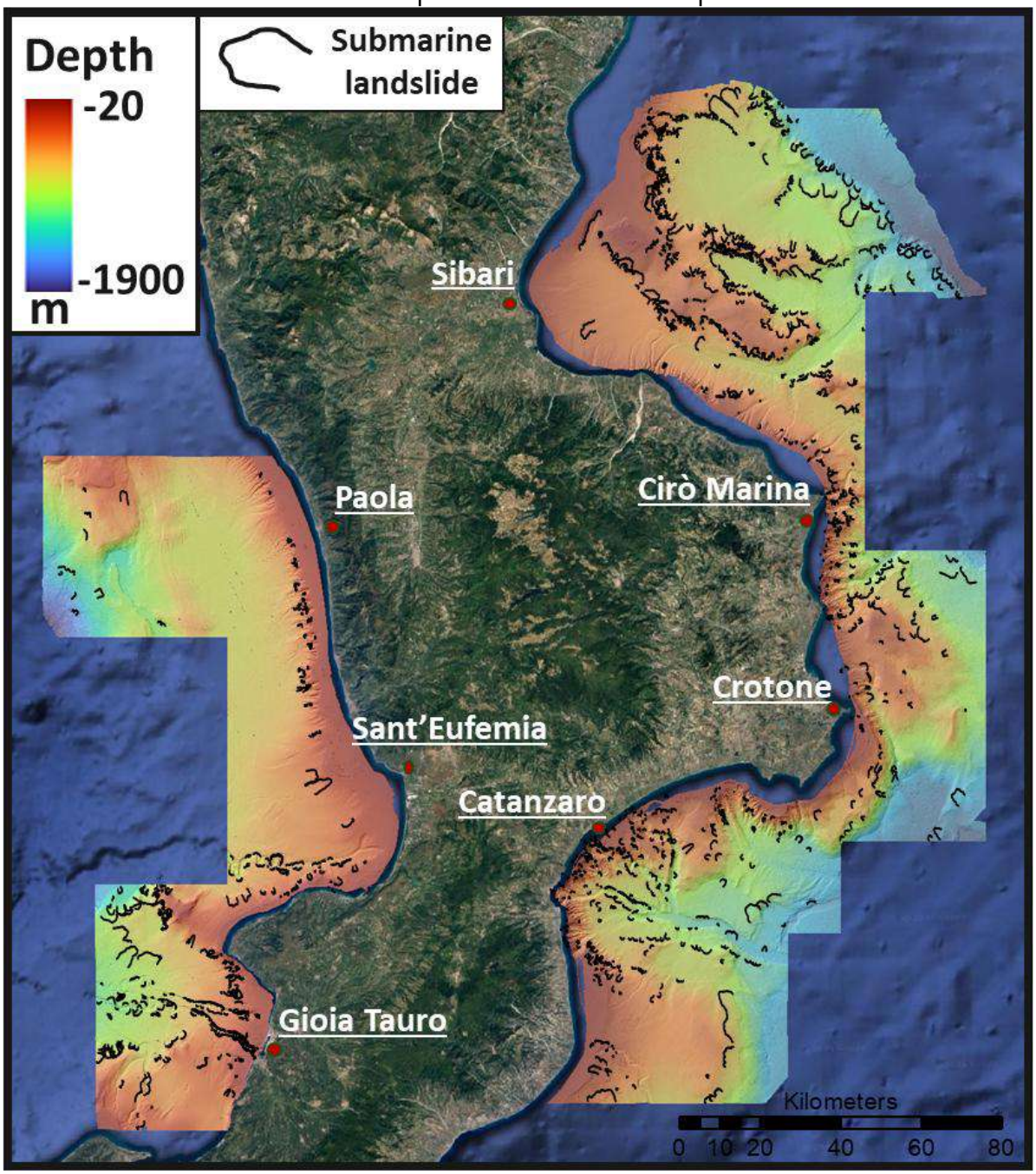

Figure 8 Map of the study area shows the digital elevation model (bathymetry) and mapped submarine landslides.

To construct the WoE model, a set of predictor layers representing potential predisposing factors for submarine landslides was defined. In the case of the Calabria region, the following eight layers were selected as input variables:

- ***Digital Elevation Model (DEM)***
- ***Slope map***
- ***Planar curvature***
- ***Profile curvature***
- ***Aspect map***
- ***Distance from Earthquake***

- ***Distance from Faults***
- ***Physiographic domain***

Once the predictor layers were defined, a binary layer was created to indicate the presence or absence of submarine landslide events. This layer is essential to statistically constrain the weights assigned to each class within the WoE model.
To enhance the model's reliability and ensure it reflects the geological variability of the region; the study area was subdivided into two distinct sectors based on the structural and morphological differences of the continental margin: the Tyrrhenian Sea sector and the Ionian Sea sector. This division allows for a more regionally consistent susceptibility analysis, accounting for the contrasting tectonic and sedimentary settings that influence submarine landslide processes in each domain.

5.2.2.1 Results

The landslide susceptibility analysis resulted in the following key outputs:

- Susceptibility maps for both investigated areas
- Tables of contrast indexes
- ROC curves with AUC scores

The resulting susceptibility map clearly delineates the areas that are most affected by the selected predisposing factors, as determined by the spatial relationship between these predictors and the binary landslide inventory (presence/absence). This spatial output provides a valuable tool for identifying zones with higher likelihood of submarine slope failure, thus supporting risk mitigation strategies and seafloor planning.
The analysis of contrast values (Fig. 9a,c) revealed that, overall, both investigated sectors share the same key predictors influencing landslide susceptibility. However, differences emerge when examining the specific classes within each predictor. While the same variables drive susceptibility across the Tyrrhenian and Ionian margins, the classes associated with higher contrast values vary between the two sectors. This indicates a **notable internal variability**, likely reflecting the distinct geomorphological and geological settings of the two regions.
The developed susceptibility models demonstrate high predictive accuracy (Fig. 9b,d), as evidenced by the Area Under the Curve (AUC) values derived from Receiver Operating Characteristic (ROC) analysis. These AUC values exceed 0.75, indicating excellent model performance in distinguishing between areas prone to submarine landslides and those that are not. Such high AUC values suggest that the models have a strong capability to correctly classify both positive and negative instances, minimizing false positives and negatives. This level of accuracy is particularly noteworthy given the complex geological and morphological settings of the Tyrrhenian and Ionian continental margins. The robustness of these models underscores their reliability and effectiveness in assessing submarine landslide susceptibility, providing a valuable tool for hazard assessment and mitigation planning

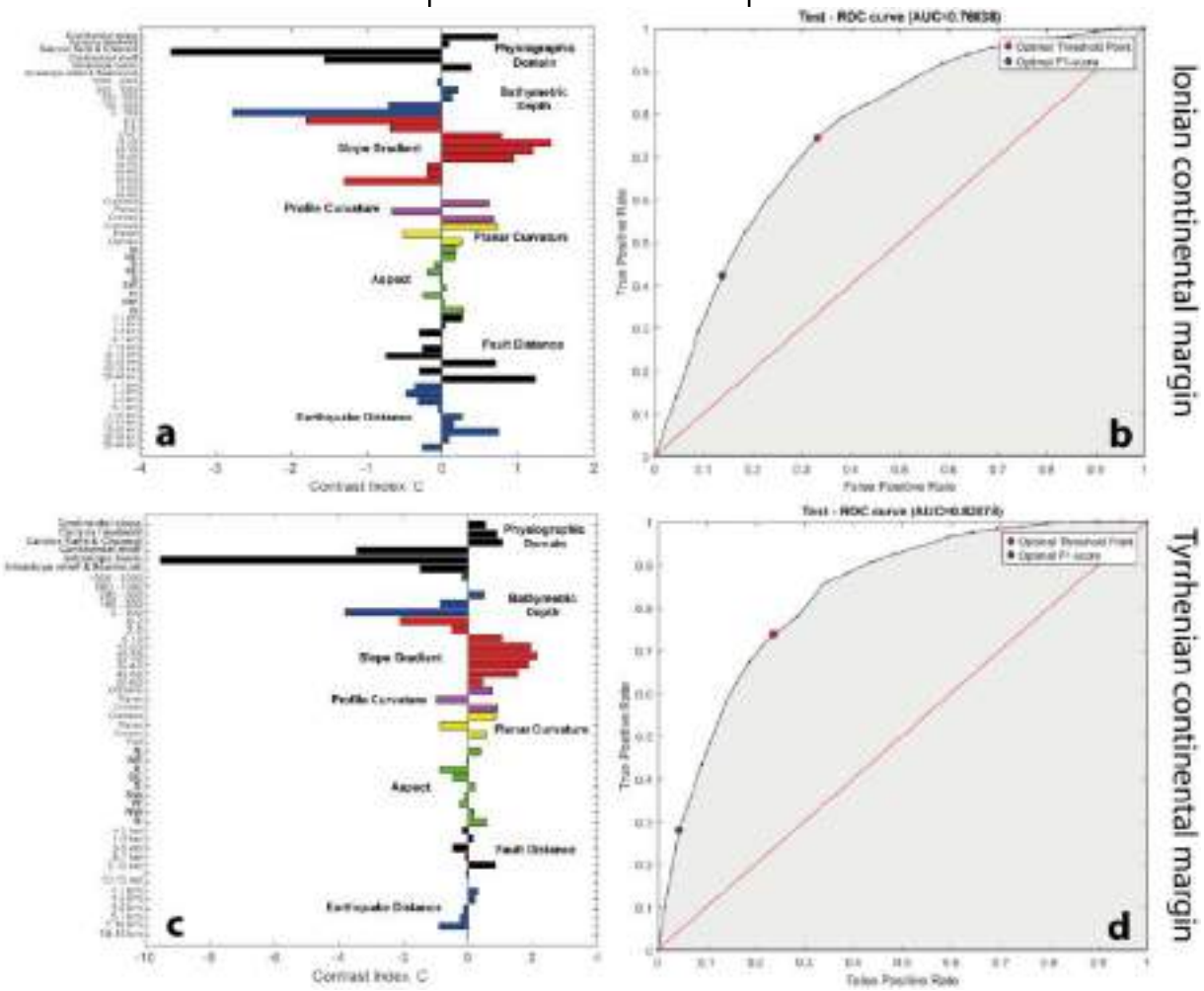

Figure 9 a-b) Contrast index and ROC curve for the Ionian submarine landslide susceptibility model (R^2 = 0.76). c-d) Contrast index and ROC curve for the Tyrrhenian submarine landslide susceptibility model (R^2 = 0.82).

5.2.2.2 Novelty, Criticalities, and Relevance/Potentiality of this Tool

This work represents the first comprehensive attempt to quantify submarine landslide susceptibility along the Calabrian Continental Margins using an extensive dataset and a robust statistical framework based on the Weight of Evidence (WoE) method. The integration of morphological and tectonic variables into a unified susceptibility model marks a significant advancement over previous approaches that often considered these factors separately or with limited spatial coverage. By applying this method to more than 12,000 km² of high-resolution bathymetric data and incorporating a landslide inventory of 1,945 events, the model provides a consistent and reproducible methodology applicable at regional scale. **Despite the strong predictive performance of the model, validated through ROC curves and contrast analysis, certain limitations must be acknowledged.** The model is static and does not account for temporal dynamics such as recurrence intervals, sedimentation rates, or hydrodynamic triggers, which are essential for understanding the timing and frequency of submarine landslides. While this approach effectively supports spatial prioritization and comparative analysis between regions (e.g., Ionian vs Tyrrhenian sectors), it does not provide an absolute assessment of slope failure probability or sediment displacement volumes. Future improvements should include time-series bathymetric or seismic data to assess slope evolution and failure thresholds in high-susceptibility zones.

The developed susceptibility model holds significant potential for marine hazard management and applied geosciences:

- **Hazard Assessment and Mitigation:** By delineating areas most prone to submarine landslides, the model supports risk-informed planning for offshore infrastructure, seafloor cables, pipelines, and environmental conservation zones.
- **Targeted Monitoring and Survey Planning:** In scenarios of limited observational capacity, monitoring efforts (e.g., geophysical surveys, sediment cores) can be focused on areas classified as highly susceptible.
- **Methodological Transferability:** The statistical framework adopted here can be easily adapted to other continental margins or submarine systems, serving as a benchmark for future susceptibility studies.

5.2.3 Local scale application

In this application, the submarine landslide susceptibility map of a shallow-water sector of the Capo D'Orlando continental margin is addressed using the WoE method. The applied methodology consisted of the identification of Landslide Initiation Points (LIPs), the representation of possible preconditioning factors, and the application of the WoE method through a specialized graphical user interface (GUI) for ground instability susceptibility analysis developed in MATLAB R2024a as part of the RETURN project (DV 2.2.6).

A detailed geomorphological analysis in an area of 415 Km^2, where bathymetric data with 10 m of resolution are available, resulted in the identification of 449 LIPs. Landslide headwalls were mapped as linear elements, based on their semicircular shape relative to nearby coalescing features. The highest points along each headwall were extracted and associated with the corresponding LIP (blue points in Figure 10). Scarps formed by erosive processes—such as turbidity currents and hyperpycnal flows capable of reshaping the seafloor and recognizable by the presence of gullies—were excluded from the model.

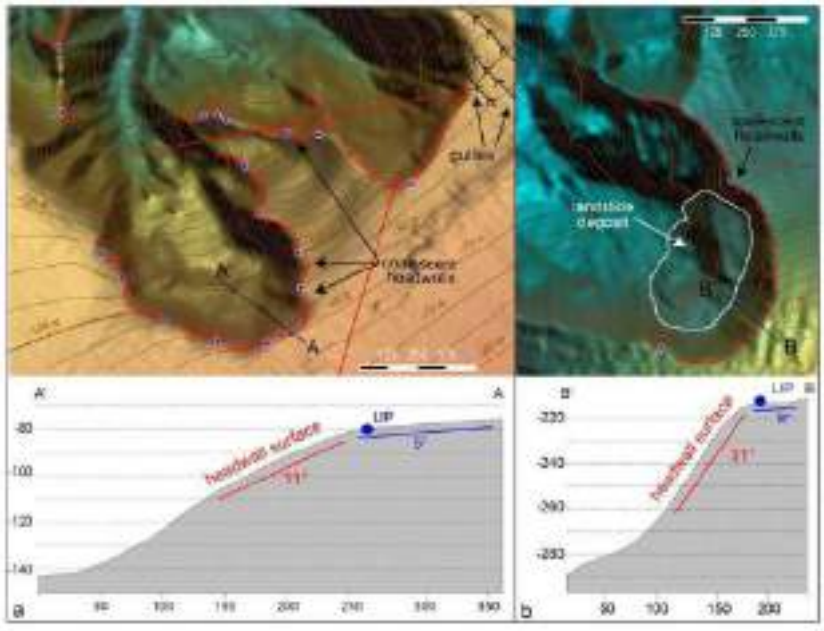

Figure 10 Landslide elements mapped in the study area, note the presence of coalescent scars and the location of the LIPs (blue point) used to approximate the slope morphology before the instability process. a) Landslides at canyon head and flank and a topographic profile crossing one of the landslide headwalls; b) Open slope landslides and a topographic profile crossing its headwall.

In this study, a set of five rasters with a 10 m grid cell size was used to account for the following preconditioning factors (Figure 11):

- ***Slope***
- ***Aspect***
- ***Simplified lithological map***
- ***Distance from river mouths***
- ***Distance from faults***

Slope and aspect, divided into 10 and 9 classes respectively, were extracted from the bathymetric data (Figure 11a-b). The simplified lithological map was created by assigning the lithology conventionally associated with different depositional environments (e.g., continental shelf, slope) and bodies (e.g., depositional terraces, transgressive deposits) mapped within the MAGIC project (Figure 11c). Distance from river mouths and faults was calculated using the Euclidean Distance tool in ArcMap (Figure 11d-e). The river-mouth distance map was based on the Italian drainage network and divided into five classes with 2 km intervals. Faults were extrapolated from METIQ Sheet 5 (METIQ Working Group, 2023), the CARG Patti Sheet 599 (Catalano et al., 2013), and, for the western part of the Capo D'Orlando continental margin, through interpretation of available seismic profiles (Gamberi et al., 2025, in preparation). Distances from faults were also divided into five classes with 1 km intervals.

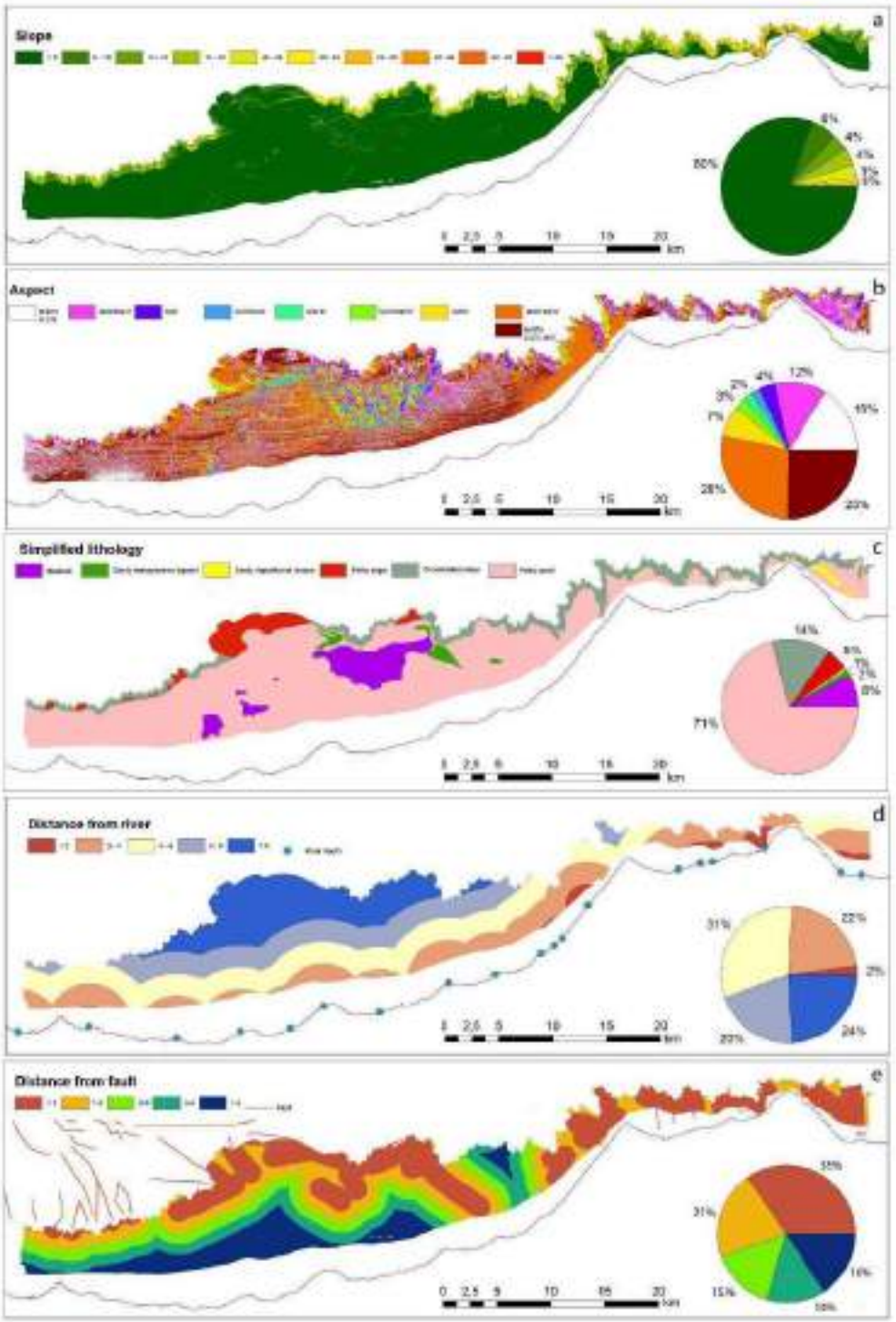

Figure 11 Preconditioning factors of the study area subdivided into their relative classes and a pie chart with the percentage of each class area; a) slope; b) aspect; c) Simplified lithology, d) Distance from river mouth; e) Distance from fault.

5.2.3.1 Results

The main results are the contrast values of the preconditioning factor classes and the resulting susceptibility map. The relative weight of the different preconditioning factors in the instability process can be understood by examining the bar plots in Figure 12a.

The classes showing the highest correlation with shallow-water landslides are:

- Slopes ranging from 5° to 15°
- Slopes oriented downcurrent with respect to the longshore currents (primarily towards NE, E, N — 0°–22°)
- Sandy depositional terraces and consolidated slopes
- Distance from rivers < 2 km
- Distance from faults < 1 km

According to the contrast index values, the most relevant factor for landslide occurrence is slope, followed by distance from rivers, distance from faults, simplified lithology, and aspect (Fig. 12a).

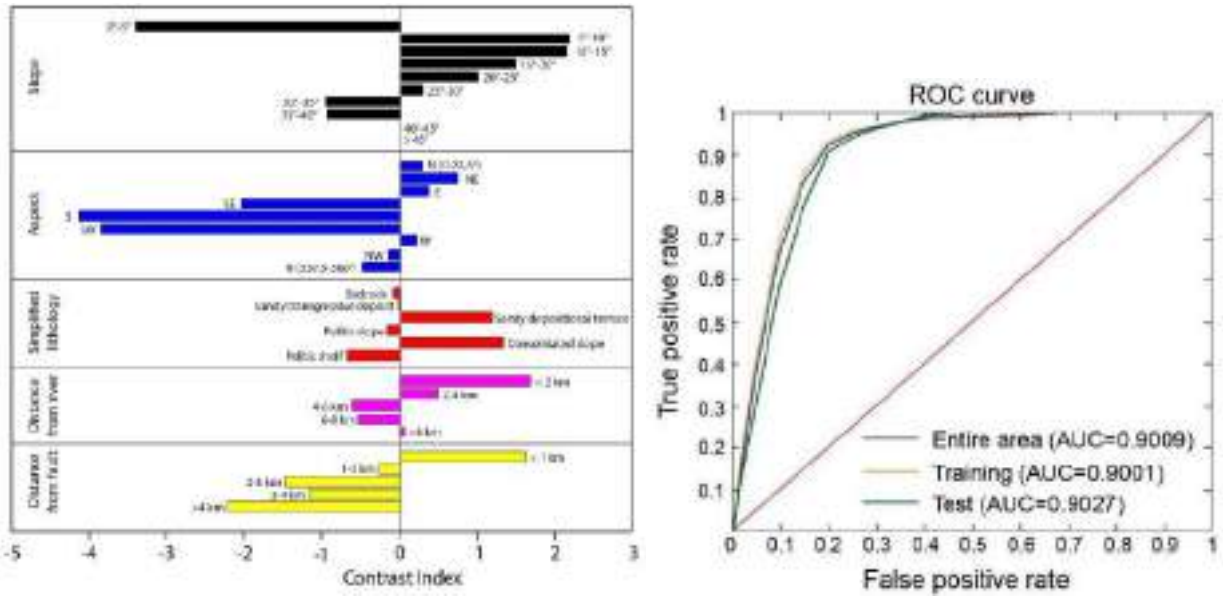

Figure 12 a) Bar plots showing the contrast of each class of the preconditioning factors related to LIPs.b) ROC curves and relative AUC of the test, training and entire area.

The values of susceptibility of the final map were grouped in 5 classes (Very low, Low, Moderate, High and Very High). The cut-off values of the susceptibility classes are set using Natural Breaks: Very Low: < 0.10, Low: 0.10 - 0.30, Moderate: 0.30- 0.60, High: 0.60- 0.80, Very High: > 0.80 (Fig. 13). The WoE method provided AUC values of 0.9027 for the test, 0.9001 for the training and 0.9009 for the entire area, indicating a good discriminating power of the model (Fig. 12b)

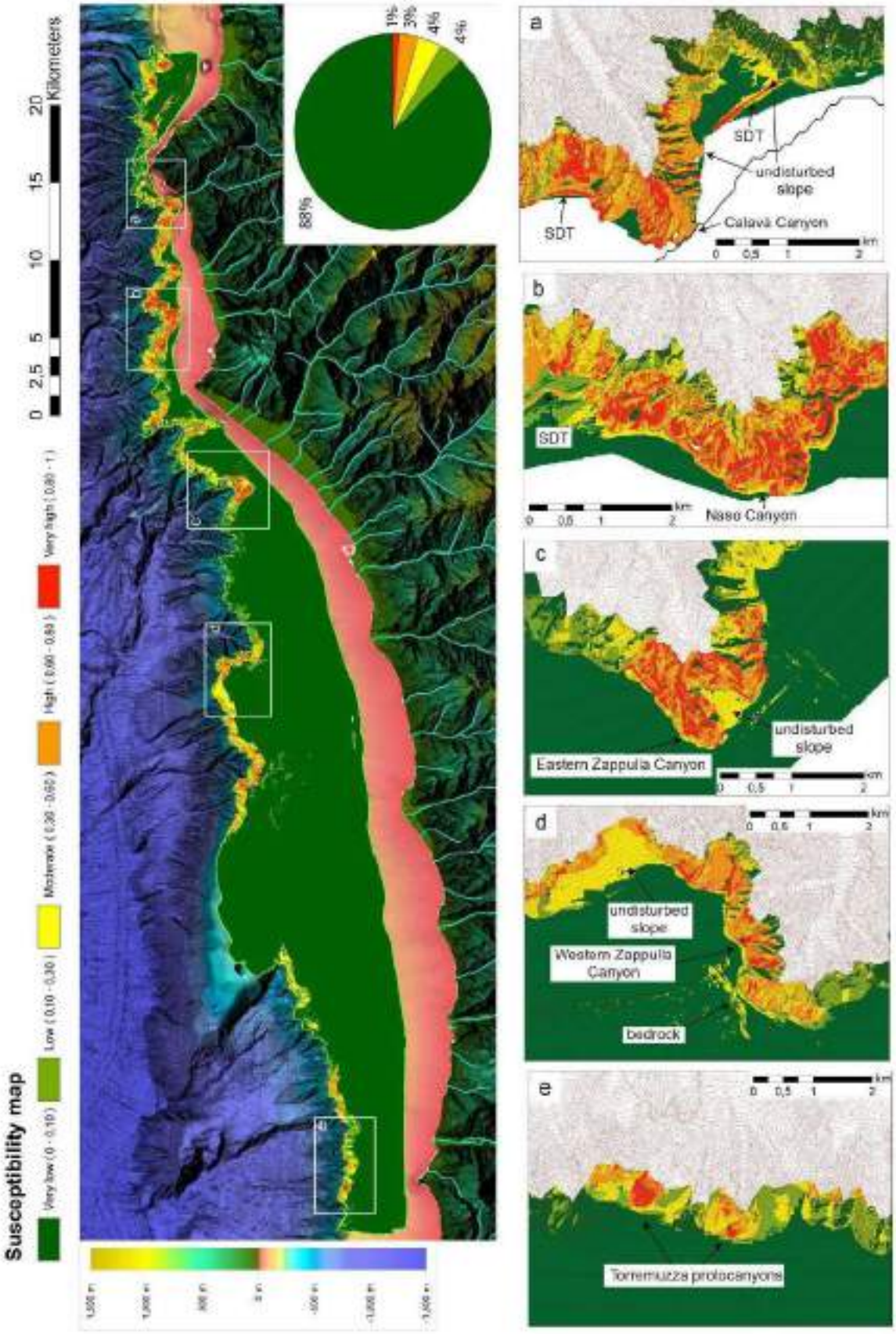

Figure 13 Susceptibility map of the shallow-water portion of the Capo D'Orlando continental margin and pie chart with the percentage of the area of the different classes. Inserts (a, b, c, d, e) contain zoom of selected areas of the susceptibility map. The high resolution of the map allows the recognition, inside

the single canyon or slope portion, of areas with different degrees of susceptibility. Contours at interval of 10m

5.2.3.2 Novelty, Criticalities, and Relevance/Potentiality of this Tool

Submarine landslide susceptibility analyses are rare and mostly developed for open-slope landslides in deep-water environments. However, landslide scars are an almost ubiquitous feature at shelf edges, particularly in active margins carved by submarine canyons. This work represents the **first attempt to quantify the most favourable conditions for generating shallow-water landslides resulting in a detailed submarine landslide susceptibility map in a shallow-water sector of a continental margin**.

The described approach is **not time-consuming**, as it is based on accessible preconditioning factors that can be easily extracted from **existing national-scale data**. Our approach resulted in a reliable model (AUC = 0.9), indicating that it can be applied to obtain preliminary susceptibility assessments in other shallow-water sectors characterized by limited databases representing a common scenario in the submarine environment. Applying this approach to other study areas could consolidate the findings of this work, providing insights into the most important factors that generally predispose slopes to instability.

The main limitation of this work lies in the **absence of direct measurements** acquired in the study area. The preconditioning factors used serve as proxies for geological processes that have not been directly measured (e.g., sedimentation rate, longshore currents) and the simplified lithological map is based on morpho-bathymetric interpretation. Nevertheless, the analysis can be easily updated if new data are acquired.

Within the framework of the RETURN project, our approach can support the production of shallow-water susceptibility maps, representing the first step in toolchains simulating the effects of instabilities on coastal infrastructures. Moreover, this approach may be useful for selecting specific areas for more detailed site investigations required to support physically based slope stability analyses.

5.3 Factor Of Safety (FOS) of submerged area linked to presence of Active Fluid Seepages (AFS)

This tool can be used to identify potential submarine landslide hazards, linked to submarine fluid flow vents and/or emission fields near coastal area, to determine risk management strategies, allowing prioritization of monitoring and mitigation efforts in areas where high susceptibility coincides with significant coastal exposure (infrastructure and/or communities). In our study we analyse submerged pockmark located in Palermo offshore (Fig. 14)

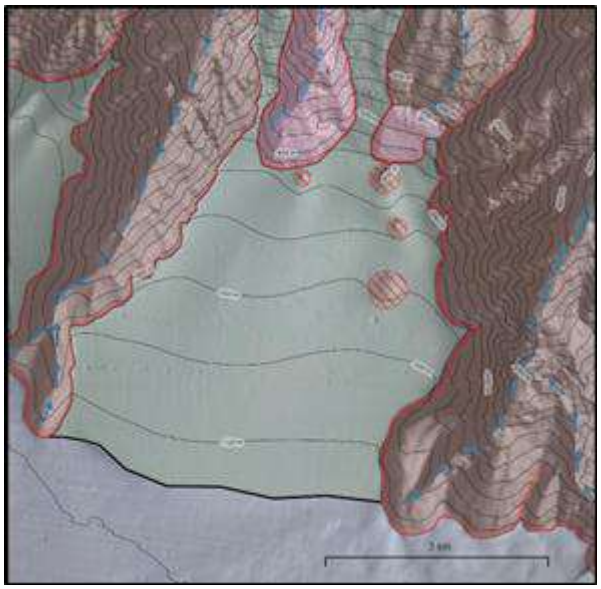

Figure 14 Case study located in the offshore of Palermo Gulf (Sicily, Italy). The red circles (in the map zoom on the right) indicate the areas of fluid seepage (Pockmark); the black line represents the coastline.

5.3.1 Method

The methodological approach is based on the analysis of morpho-bathymetric data for the identification and plan mapping of areas affected by fluid rising and the interpretation of high-resolution seismic profiles converted into geological profile, to measure the thicknesses of geological bodies potentially affected by landslide movements and the slopes of potential sliding surfaces. These studies allow us to recognize and reconstruct the bottom of a weak layer (Fig. 15) that promotes the formation of landslides.

The instability is assessed by applying a geotechnical Factor Of Safety (FOS) model from the literature (Noda et al., 2013; Sultan et al., 2004), appropriately modified to consider the fluid pressure in the area affected by fluid rise, whose formula is:

$$FOS_{mod} = \frac{\left(\gamma' h \cos^2 \alpha - \frac{10^6 h S}{200} - \Delta u_{AFS}\right) \tan \varphi + c}{\gamma' h \sin \alpha \cos \alpha}$$

where (data input):

- γ' = Submerged unit weight of sediment.
- h = Thickness of sedimentary body.

- α = Angle of slope of sedimentary body bottom.
- φ = Friction angle of sediment.
- c = Cohesion of sediment.
- S = Sedimentation rate.
- Δu_{AFS} = Excess pore fluid pressure in intra-area of emissive vent.

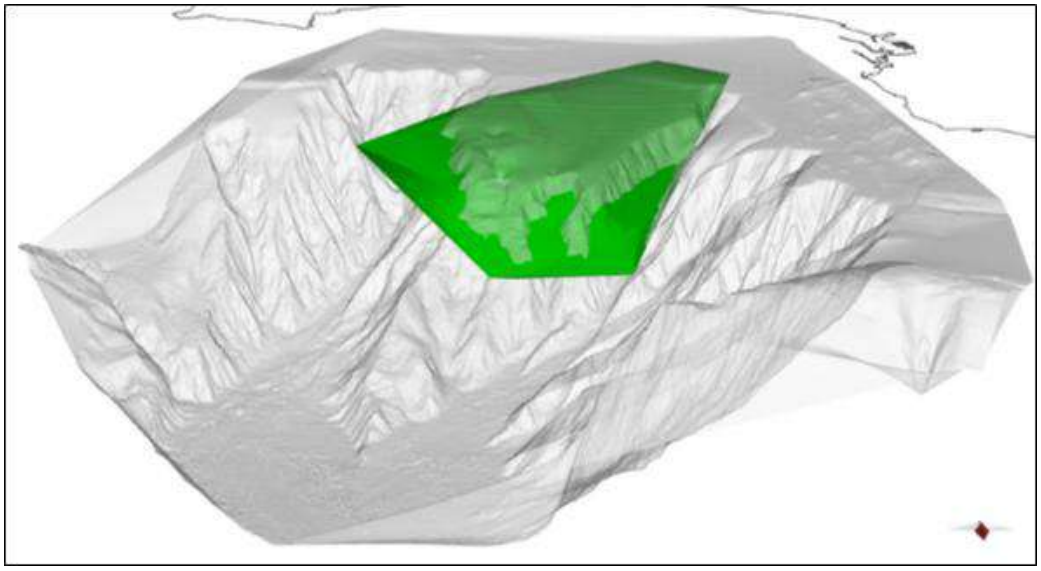

Figure 15 3D model of potential weak layer surface (green) reconstructed by seismic profiles interpretation (MOVE geological modeling software).

All input parameters are site-specific but, given the low lithological and geomechanical variability within the single emission points, γ', φ, c and S can be assumed constant (based on literature data or direct measurements if available); on the contrary, h and α, being able to present considerable variability, must be measured from morphobathymetric and seismic data. Regarding the production of the raster related to Δu_{AFS}, whose value is not directly measurable, an iterative process was used to solve the equations. This process involved varying this parameter within a predefined range (based on literature data), with a step size established beforehand (*brute force* approach).

After rasterizing each input parameter, FOS_{mod} equation is solved with the "raster calculator" tool in a GIS environment (Fig. 16).

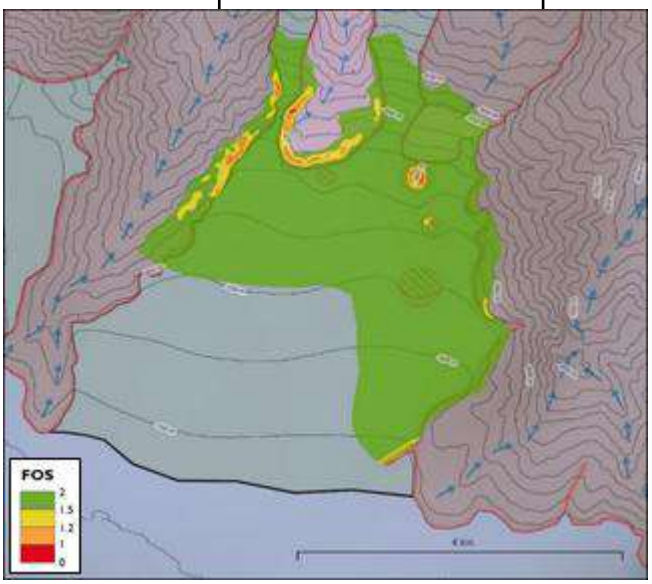

Figure 16 FOSmod map obtained by imposing the overpressure (ΔuAFS) of 150 kPa (see text for discussion).

5.3.2 Results

This approach enables the study of the controlling parameters for the slope's evolution. In the model proposed, the pore overpressure in fluid seepage area (Δu_{AFS}), and its threshold value, determines the equilibrium of the slope.

The susceptibility classification by FOS_{mod} values is taken by 3 ranges of values (Fig.16):

1. Stability condition threshold for $FOS_{mod} \geq 1.2$.
2. Attention range for $1 \leq FOS_{mod} < 1.2$.
3. Gravitative instability threshold for $0 < FOS_{mod} < 1$.

5.3.3 Novelty, Criticalities, and Relevance/Potentiality of this Tool

This tool represents a method of quantifying landslide susceptibility in the presence of fluid seepages from the seabed from local to areal sector according to the size of the emission point.

The limitation of the model may be related to the low/poor availability of site geotechnical data due to the difficulty and cost of acquisition.

Future improvements should include time-series bathymetric and seismic data, core sampling and installation of piezometers to capture evolution rates in high-susceptibility areas and to calibrate the model on the specificity of the site.

The developed tool offers significant potential for hazard management applications:

- **Hazard assessment and mitigation** - By identifying areas with high landslide susceptibility, the tool provides valuable information for coastal zone management and infrastructure planning.

- **Prioritization of monitoring efforts** - Limited marine monitoring resources can be directed to the most sensitive areas identified by the tool.

- **Methodological framework** - The approach establishes a repeatable methodology that can be adapted to other areas.

- **Integration with cascading hazard models** - The susceptibility assessment provides a basis for modelling cascading hazards such as landslide-triggered tsunamis.

5.4 Landslide-Tsunami propagation

5.4.1 Method

The LANDSLIDE-TSUNAMI tool provides an estimation of the maximum tsunami amplitude on the coast, starting from the geomorphological characteristics of the landslide generating the waves. The tool consists of a parametric expression, obtained by correlating a combination of some features describing the source (volume, initial slope angle, depth, distance from the coast) to a quantity describing the tsunami impact on the coast, i.e., its maximum amplitude.

The basic equation is:

$$\eta = A(V^{\varepsilon_V} \cdot D^{\varepsilon_D} \cdot d^{\varepsilon_d} \cdot sin\theta^{\varepsilon_\theta}) + B \qquad (5.4.1)$$

Where the input quantities are: V, initial slide volume, measured in m^3; D, initial slide barycenter depth (m); d, distance between the slide barycenter and the coast (m); θ, average slope of the scar (°). The output, η, is the maximum tsunami amplitude at the coast (in m).

The exponents ε_V, ε_D, ε_d, ε_θ, and the parameters A and B are retrieved through a procedure that is explained in section 5.4.1.1, producing the results reported in Table 1 for two different contexts, open slope and canyon head.

Quantity	Parameter	OPEN SLOPE	CANYON HEAD
Volume	ε_V	1.0	0.9
Depth	ε_D	-1.2	-0.5
Distance	ε_d	-0.5	-1.2
Slope	ε_θ	1.1	0.5
Best fit	A	0.01096	0.10543
Best fit	B	-0.01328	0.00280
Uncertainty	ΔA	0.00025	0.00071
Uncertainty	ΔB	0.03336	0.00166

Table 1 Values for the coefficients governing Eq. 5.4.1 obtained for the two different contexts (open slope and canyon head) through the best-fit procedure described in section 5.4.1.1.

The distinction between the two environments follows the approach adopted in the identification and characterization of the gravitational instabilities in the submarine context. The values obtained and reported in Table 1 suggest that in both cases there is a direct correlation of the tsunami amplitude with volume and slope (positive exponents), and an inverse correlation with depth and distance from the coast (negative values). Such findings sound perfectly reasonable, since it is well known, for example, that deeper mass movements induce smaller waves than shallower ones, or that steeper slopes, inducing higher initial acceleration, generate higher tsunamis (for landslide-tsunami features see Løvholt et al., 2015; Yavari-Ramshe and Ataie-Ashtiani, 2016).

One of the most interesting aspects of parametric expressions like 5.4.1 is that they quantify the contribution of each input quantity, characterizing the landslide source, on the tsunami generation: the higher is the absolute value of an exponent, the more sensitive is the output to the changes of the respective feature. In the specific, we can observe from Table 5.4..1 that in the open slope context depth, slope and volume play the most relevant role, with similar exponents, while distance has a secondary effect; in canyon head environment, the last is the quantity more efficient on the tsunamigenesis, together with the volume, whereas depth and slope have a smaller impact.

5.4.1.1 Description of the parametric relation construction

The values reported in Table 1 have been obtained by means of a procedure involving some steps, that can be schematized and described as follows:

i) *Scenarios definition.* One reference area has been selected and investigated for each context: for the open slope, the Assi landslide complex (Ionian coast of Calabria, see Ceramicola et al., 2014 for further description), consisting of a sequence of collapses occurring along the same margin at different depth and with different volume scales (see Fig. 17 and Table 2); as to the canyon head environment, the Capo d'Orlando offshore (Tyrrhenian coast of Sicily), characterized by numerous canyons that in some cases can reach the coast (Fig. 18), with several scars and deposit accounting for mass instability processes. In both regions, a set of three submarine landslide scenarios has been defined (see Fig. 17 and Fig. 18 for the initial positions of the landslides, Table 2 for their geomorphologic features). For Assi scenarios, volume, depth and distance span larger ranges than Capo d'Orlando one, where on the contrary a larger variability of the initial slope is accounted for.

Area	Scenario	Volume ($10^6\ m^3$)	Depth (m)	Distance (m)	Slope (°)
Assi (Open slope)	1	56.3	276	8089	3.7
	2	702.0	572	13070	3.5
	3	1919.8	966	21101	2.8
Capo d'Orlando (Canyon Head)	1	6.2	267	8201	19.6
	2	3.6	67	3057	22.6
	3	3.2	144	2443	24.7

Table 2 Geomorphologic features of the scenarios investigated.

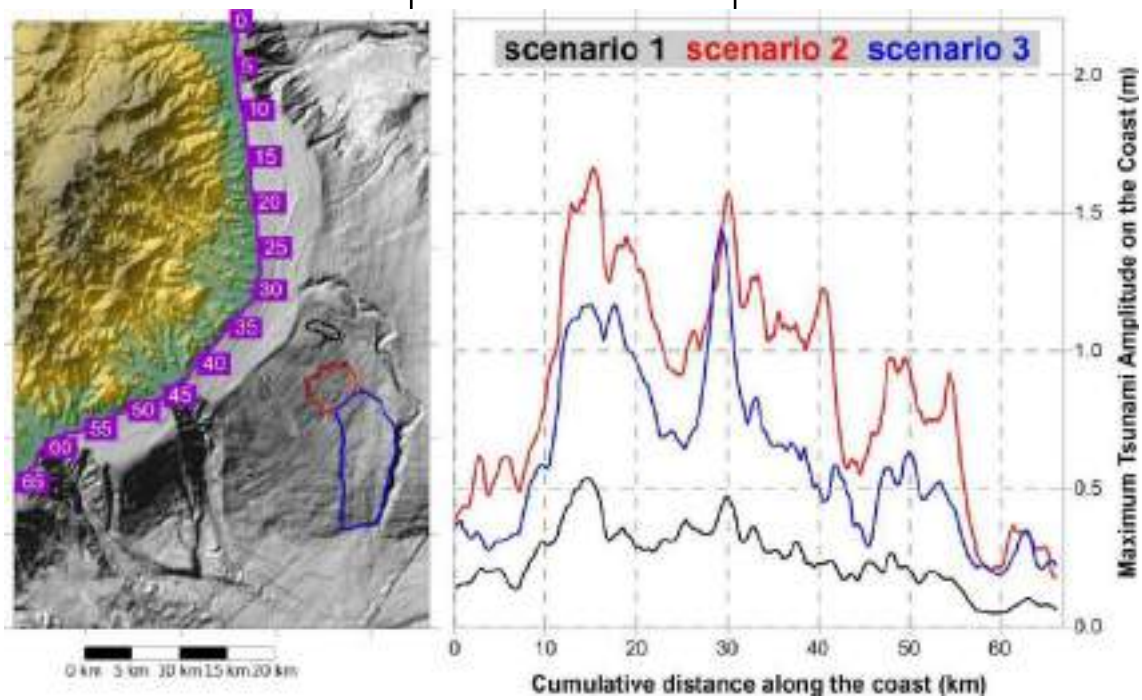

Figure 17 Left panel) map of the Ionian Calabria coastal stretch object of this investigation. The black, red and blue boundaries mark respectively scenarios 1, 2 and 3 of the Assi landslide complex. The purple labels indicate the cumulative distance along the coast. Right panel) Maximum tsunami amplitude on the coast vs cumulative distance along the coast for the three landslide scenarios (1-black, 2-red, 3-blue, respectively).

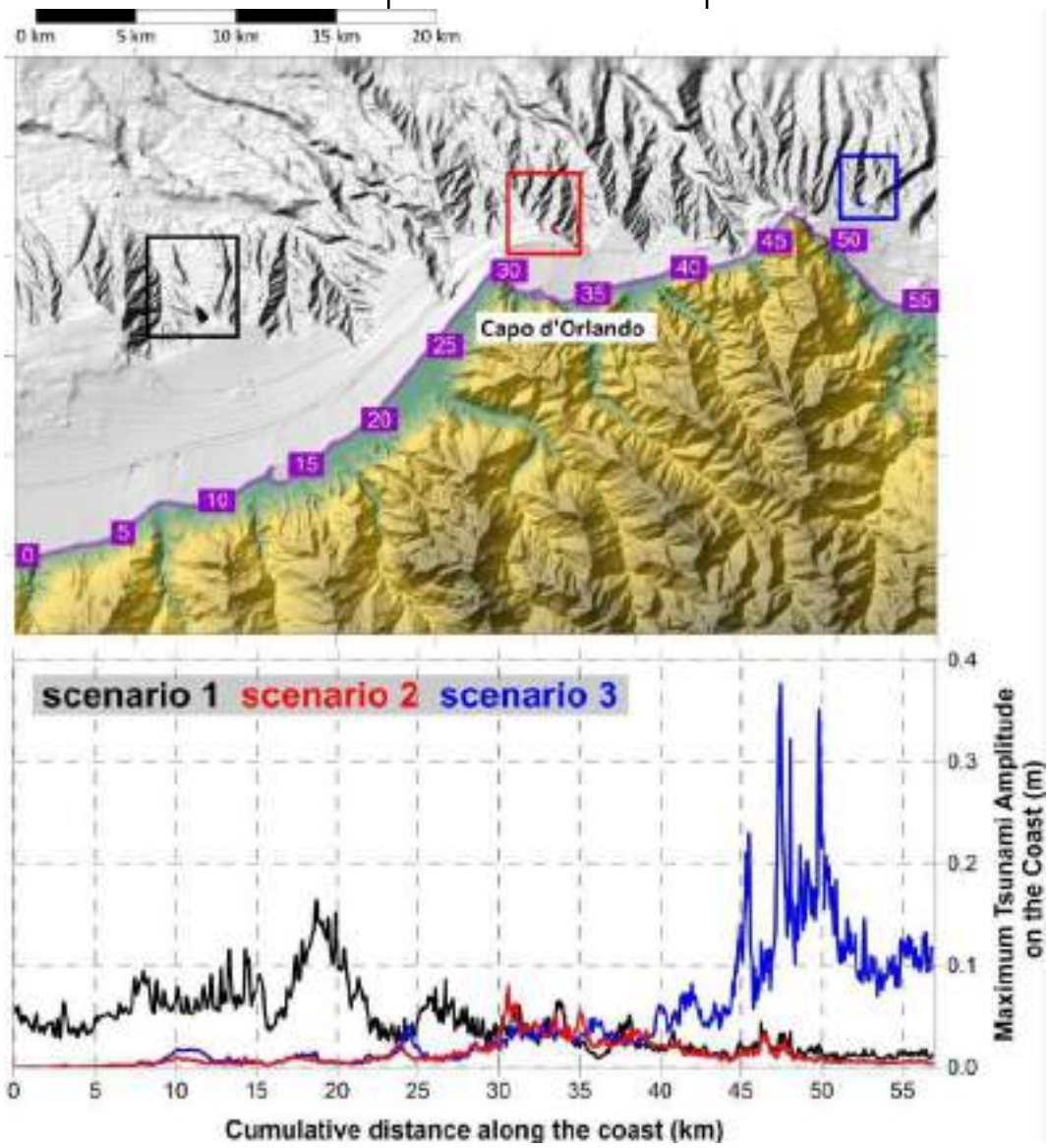

Figure 18 Upper panel) map of the northern Sicily coastal stretch around Capo d'Orlando. The black, red and blue rectangles mark the scenario areas respectively for cases 1, 2 and 3. The purple labels indicate the cumulative distance along the coast. Lower panel) Maximum tsunami amplitude on the coast vs cumulative distance along the coast for the three landslide scenarios (1-black, 2-red, 3-blue, respectively).

ii) *Numerical simulations*. For each scenario, the respective landslide dynamics has been simulated, and the ensuing tsunami mimicked by means of a sequence of numerical codes tested and applied in many cases of landslide-tsunamis (see Zaniboni et al., 2021; Gasperini et al., 2022; Gallotti et al., 2023; Zaniboni et al., 2024 and references therein). The maximum tsunami distribution along the coast is reported in Fig. 17 (right panel) and Fig. 18 (lower panel) respectively for the Assi and the Capo d'Orlando scenarios.

iii) *Additional scenarios*. To enlarge the results dataset used to build the parametric expression, the initial thickness of each landslide scenario has been multiplied by a set of six factors spanning the range $[0.25 - 2]$, obtaining a total of 21 scenarios, for which the whole numerical routine previously cited has been applied. This sensitivity analysis aimed at providing insights on the influence of factors characterizing the landslide on the tsunami generation.

iv) *Parametric correlation*. The contributions of the parameters describing the landslide source on the tsunami generation is then evaluated with Eq. 5.4.1, searching for the combination of factors (in the specific, here, their

exponents) providing the best-fit correlation with the reference values, that are represented by the maximum wave elevation of each scenario on the coast. This procedure produces also an estimation of the best-fit parameters and , with the respective uncertainty.

5.4.1.2 Uncertainty quantification

According to the theory of uncertainty propagation, the error on the quantity $y = y(a, b, c, \dots)$ can be obtained knowing the specific uncertainties of each quantity (Δa, Δb, $\Delta c \dots$) through the expression:

$$\Delta y = \left|\frac{\partial y}{\partial a}\right| \Delta a + \left|\frac{\partial y}{\partial b}\right| \Delta b + \left|\frac{\partial y}{\partial c}\right| \Delta c + \dots \quad (5.4.2)$$

Writing then Eq. 5.4.1 as

$$\eta = A \cdot x + B$$

the absolute error on the output is, according to Eq. 5.4.2:

$$\Delta \eta = A \cdot \Delta x + x \cdot \Delta A + \Delta B \quad (5.4.3)$$

Where x is the quantity:

$$x = V^{\varepsilon_V} \cdot D^{\varepsilon_D} \cdot d^{\varepsilon_d} \cdot (sin\ sin\ \theta)^{\varepsilon_\theta} \quad (5.4.4)$$

The only unknown term in Eq. 5.4.3 is Δx, the uncertainty on x, that depends on the error associated to each input quantity. Invoking again Eq. 5.4.2, the relative error on can be written as:

$$\frac{\Delta x}{x} = |\varepsilon_V| \frac{\Delta V}{V} + |\varepsilon_D| \frac{\Delta D}{D} + |\varepsilon_d| \frac{\Delta d}{d} + |\varepsilon_\theta| \frac{\Delta \theta}{tantan\ \theta}$$
(5.4.5)

To simplify the last term of Eq. 5.4.5, one can consider $tan\ \theta \approx \theta$ obtaining the relative error on the slope angle, $\frac{\Delta \theta}{\theta}$, which can be considered an optimal approximation for small angles (i.e. $\theta < 20°$).

While ΔA and ΔB come from the best-fit analysis and do not change when applying these formulas, ΔV, ΔD, Δd and $\Delta \theta$ depend on the degree of knowledge of the slide features. As an example, an error of 10% on each input quantity provides a relative uncertainty of 38% for open slopes, and 31% in canyon heads. This must be combined with the uncertainties on ΔA and ΔB according to Eq. 5.4.3 to produce the final evaluation of $\Delta \eta$.

5.4.1.3 Range of values for the input quantities

The empirical expression 5.4.1 provides the maximum tsunami amplitude η without any control on the output: it can then reach unrealistic values with small distances from the coast or with huge volumes, for example. To prevent such occurrence and to avoid questionable or excessive tsunami amplitudes, for each input quantity a range of value is provided in Table 3: upper limits for volume and initial slope, lower thresholds for depth and distance.

		OPEN SLOPE	CANYON HEAD
V	Volume ($10^6\ m^3$)	< 2000	< 20
D	Initial depth (m)	> 200	> 20
d	Distance from the coast (m)	> 1000	> 100
θ	Initial slope (°)	< 20	< 45

Table 3 Range of possible values for the input quantities of Eq. 5.4.1.

These are mainly based on reasonable and arbitrary assumptions: for example, it is extremely unlikely for a mass of to detach in shallow water or to be placed very close to the coast. In the open slope context, volumes bigger than the upper limit provided (2 km^3) are not unusual, such as different values for depth and distance: the limits reported in Table 3 should be assumed then with some flexibility. Even better, a combination of thresholds should be implemented: this would require a larger database of events and further considerations on the combined effects of the input quantities that are out of the scopes of this study. Canyon head thresholds, on the contrary, are quite standard and can be considered tighter. However, when simply introducing these limit values in Eq. 5.4.1, a maximum tsunami amplitude of almost 47 m is obtained in the open slope context, and 37 m for the canyon head environment.

5.4.2 Results

Eq. 5.4.1 provides a rapid assessment of the expected maximum tsunami amplitude η. Its formulation contains also the distance from the source to the shoreline, meaning that it can be used to assess the tsunami amplitude for different points on the coast: the landslide volume, the initial landslide slope and the landslide depth are the same, while the distance from the landslide center of mass changes for each of them.

To assess its efficacy in different cases, expression 5.4.1 is here applied to some cases of submarine landslides, whose geometric characteristics are reported in Table 4 Besides two scenarios already described (Assi – case 2 and Capo d'Orlando – case 3), two further events are studied, one for each context; for the open slope environment, the Southern Twin Slide in the Gela Basin, south of Sicily, one of the numerous submarine collapses characterizing the Gela Basin Margin slope, involving a volume of almost half (for more details about the complex mass transport dynamics of the area, see Kuhlmann et al., 2017; numerical simulation of the landslide and the tsunami are reported in Zaniboni et al., 2021); as to the canyon head, a scenario of submarine collapse in the Vado Ligure offshore (Ligurian Sea coast, west of Genoa), at the head of one of the numerous canyons curving the Ligurian Margin. This scenario presents characteristics comparable to the Capo d'Orlando case, apart from the depth.

Area	Context	Volume (10^6 m^3)	Depth (m)	Distance (m)	Slope (°)
Assi	OS	702.0	572	13070	3.5
Gulf of Gela	OS	428.7	427	17921	5.3
Capo d'Orlando	CH	3.2	144	2443	24.7
Vado Ligure	CH	2.2	530	2560	21.6

Table 4 Geomorphologic features of the cases illustrated in Fig. 19. In the context column, OS stands for open slope, CH for canyon head.

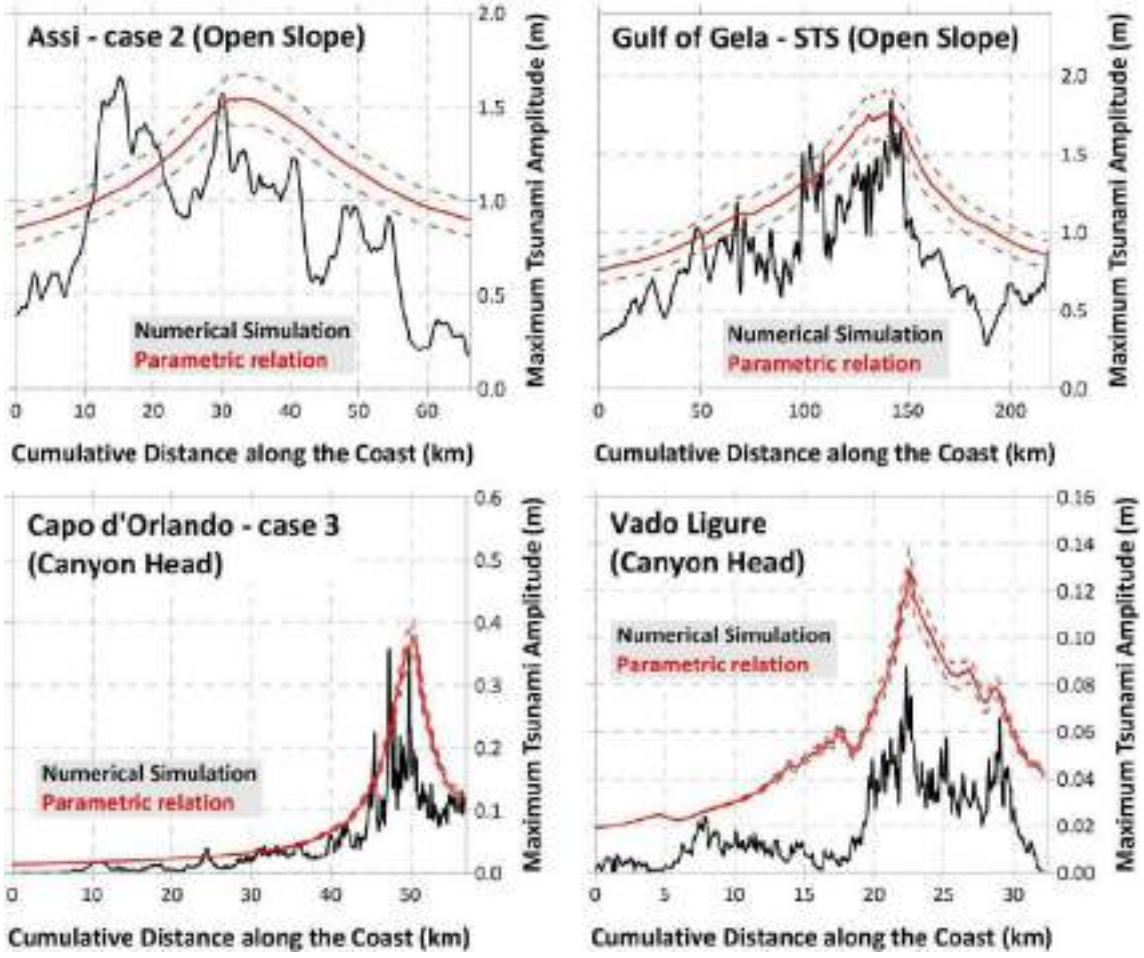

Figure 19 Maximum tsunami amplitude along the coast obtained through the parametric expression 5.4.1 (red continuous line) with respective uncertainty (red dashed lines) compared to the output of the numerical simulations (black line), in four different landslide-tsunami scenarios: Assi, scenario 2 (upper left panel), Southern Twin Slide in the Gulf of Gela (upper right panel), Capo d'Orlando, scenario 3 (lower left panel), Vado Ligure (lower right panel).

Figure 19 reports the results obtained for the coastal points applying Eq. 17 with the parameters listed in Table 1 and Table 4 (red lines, with uncertainty marked by the dashed-red lines), compared to the amplitudes obtained through the numerical simulations (in black). The uncertainty is computed through Eq. 5.4.3 and Eq. 5.4.5, with relative error on the input quantities set to 10% in the open slope context, and 30% for the canyon head ones. The obvious consequence of the use of Eq. 5.4.1 is that the peak of maximum tsunami amplitude on the coast will always coincide with the point closer to the landslide source: this does not necessarily fit the maximum amplitude obtained through the simulations, as it can be seen for Assi and Capo d'Orlando cases. Moreover, a general overestimation can be observed, apart from single points where nonlinear coastal effects prevail, generating local maxima that can't be captured by simple parametric expressions. In general, the decay of the tsunami amplitude when increasing the distance from the source can be remarked.

5.4.2.1 Comparison with other parametric expressions

Empirical formulas correlating the tsunami amplitude to the respective landslide source are already present in the scientific literature. To assess the efficacy of the equation described here and compare it to other expressions, some of these have been selected and applied to the four scenarios described in the previous section.

The first one comes from Rahiman and Pettinga (2006), and provides both the wavelength λ and the maximum tsunami amplitude at the coast (here η_{RP}):

$$\lambda = 3.87 \cdot \left(\frac{bD}{sin\,\theta}\right)^{0.5} \tag{5.4.6a}$$

$$\eta_{RP} = 0.224 \cdot T \cdot \left(\frac{w}{w+\lambda}\right) \cdot [(sin\,\theta)^{1.29} - 0.746 \cdot (sin\,\theta)^{2.29} + 0.170 \cdot (sin\,\theta)^{3.29}] \cdot \left(\frac{b}{D}\right)^{1.25} \tag{5.4.6b}$$

Where b is the length of failure mass perpendicular to the margin, D is the initial water depth at the middle of failure mass, θ is the mean slope of failure scar, T is the maximum initial mass thickness normal to the slope, and w the initial width of failure mass parallel to margin.

Another very popular expression comes from Watts et al. (2005), where the maximum tsunami amplitude (denoted here as η_W) is given by:

$$\eta_W = 0.0286 \cdot T \cdot [1 - 0.75 \cdot sin\,\theta] \cdot \left(\frac{b \cdot sin\,\theta}{D}\right)^{1.25} \tag{5.4.7}$$

Where the quantities included have the same meaning of the previous expression.

A more recent parametrization has been provided in Zengaffinen-Morris et al. (2022), from which the tsunami amplitude η_{ZM} is obtained as:

$$\eta_{ZM} = 0.073 \cdot \left[\frac{V \cdot (sin\,\theta)^2}{D^2 \cdot F^{0.3}}\right]^{0.89} \tag{5.4.8}$$

where V is the landslide volume and F the landslide safety factor, obtained through the study of the mass instability.

It is straightforward to notice that in Eq. 5.4.1 most of the input quantities are common to the other parametric formulas. In most cases the higher control on the tsunami generation is provided by the slope, with exponents that are quite like Eq. 5.4.1. The main and most noticeable difference lays in the use of the distance from the coast, that has never been considered in the previous formulation and that can affect considerably the wave amplitude at the coast: indeed, the tsunami amplitude can be reduced significantly by the distance, both for energy dissipation and for simple geometric reasons (i.e., the same tsunami front distributes on larger areas with increasing time).

Moreover, the new formulation allows one to estimate the tsunami amplitude for different points on the coast, accounting for their distance from the source, while all the other approaches provide the same value for all of them. Considering the four scenarios previously introduced, and inserting the input quantities in these empirical formulas, it is possible to assess the expected maximum tsunami amplitude according to each expression, comparing them to the values retrieved from the numerical simulations. Results are listed in Table 5.

	Assi (OS)	*Gela (OS)*	*Capo d'Orlando (CH)*	*Vado Ligure (CH)*
η_{SIM}	**1.57**	**1.84**	**0.35**	**0.09**
η_{RP} *(Eq. 5.4.6)*	0.63	2.35	1.71	0.08
η_W *(Eq. 5.4.7)*	0.61	3.44	0.92	0.27
η_{ZM} *(Eq. 5.4.8)*	0.51	1.08	1.52	0.08
η_{NEW} *(Eq. 5.4.1)*	1.50 ± 0.13	1.77 ± 0.14	0.34 ± 0.03	0.11 ± 0.01

Table 5 Comparison of the tsunami maximum amplitude on the coast obtained for the four scenarios previously described. OS stands for open slope, CH for canyon head context. η_SIM, in bold, represents the reference values, obtained by means of numerical simulations. The other rows report the outputs obtained through the empirical expressions 5.4.6, 5.4.7, 5.4.8 and 5.4.1. All values are expressed in meters.

Taking as reference the estimations obtained through the numerical simulations (upper row, in bold), it can be noted that Eq. 5.4.1 performs quite well, producing values that are close to the simulation results: if for Assi and Capo d'Orlando this is obvious (since the parametric expression has been obtained from them), for Gela and Vado Ligure the fit is really satisfying. In Assi case, all the other expressions produce a large underestimation, opposite to what happens for Capo d'Orlando; Eq. 5.4.7 overestimates the simulated values both in Gela and in Vado Ligure cases, while Eq. 5.4.6 and 5.4.8 fail for Gela case and are very accurate in Vado Ligure scenario.

5.4.3 Novelty, Criticalities and Relevance/Potentiality of this tool

Empirical formulas like 5.4.1 have the undoubted advantage to provide a rapid estimation of the expected tsunami amplitude on the coast, relying only on the knowledge of some characteristics of the landslide source. Moreover, they provide insights on the influence of the different factors describing landslides on the tsunami they generate. As shown in the previous section, the expression here also integrates the distance of the landslide from the coast, a factor that surely influences the wave impact on the coast and that has not been considered so far. This allows also to easily estimate the tsunami amplitude on different points on the coastline. There are some drawbacks, which are resumed, illustrated and discussed in the following.

In the specific of expression 5.4.1, the first criticism is of course its site-specificity, meaning that changing the setting provides very likely different estimation for the coefficients, and probably also the involvement of other quantities that are not considered in this investigation. An attempt to overcome this limitation came from the application of this approach to two different contexts: open slope and canyon head. The coefficients obtained are different (Table 1), but it is interesting to notice that their values do not differ excessively, meaning that the different input quantities contribute in a similar way to the tsunami generation, each reflecting the peculiarity of the respective context. The application of Eq. 5.4.1 to other scenarios, representing both environments but in other areas, showed satisfactory comparison with the results obtained through numerical simulations.

In both contexts presented here, expression 5.4.1 provides a rough estimation of the tsunami impact on the coast, with a general overestimation when comparing them to numerical simulations. The values obtained through its application, then, should be taken with some caution, keeping in mind that they can represent a conservative estimation of the tsunami impact: this is acceptable from the tsunami hazard assessment point of view.

In general, parametric expressions associating tsunamis to landslide features do not capture some physical processes of the landslide (which dynamics and interaction with water are not considered), nor hydrodynamic effects of the generated waves, especially non-linear ones occurring mainly in shallow water environment, close to the coast. This is particularly evident in Figure 19, in the comparison with the numerical simulations: the parametric expression can't account for local amplitude peaks, due to peculiar morphologies or other non-linear local effects (produced by canyons, river estuaries, coastal basins, resonance), that can be captured only by simulations. Eq. 5.4.1 produces simply a decreasing amplitude, in both directions, starting from the coastal point closer to the source. However, even with those limitations, parametric expressions can be of great help when several potential sources are in a particular area or context, helping in the selection of the cases which are worth of deeper investigation.

5.5 Tsunami flooding

5.5.1 Method

The tsunami flooding tool implements the Energy Method (EM), an approach described in Kriebel et al. (2017), which allows to assess the flow depth (see Table 6 for its definition, together with some tsunami metrics) and other quantities describing the tsunami flooding along a topographic transect starting from the flow amplitude at the coastline. In this method, the tsunami is approached as a constant flow entering from the coastal point, which dissipation is accounted for by means of considerations on energy conservation. This produces an ordinary differential equation (illustrated in section 5.5.1.1), solved through a numerical procedure (section 5.5.1.2), which is implemented into a MatLab script.

The tool needs in input:

- The 2D topographic profile, with representing the horizontal distance along the profile and its elevation.
- The tsunami amplitude at the coast, taken as a constant value.
- The roughness coefficient, accounting for dissipative effects on the flow during the inland flooding.

It provides as output:

- The flow depth on each point of the transect.
- The flux velocity, on each point of the transect.

This makes it possible, then, to evaluate the impact of the flux on buildings, structures and also population placed at different locations along the profile.

Term	Definition
Runup	Maximum topographic elevation reached by the water at the end of the inundation
Inundation	Horizontal distance of tsunami penetration from the shoreline
Maximum inundation	Inundation at the runup point
Flow depth	Thickness of the water column above the ground during the inundation
Inundation height	Sum of the flow depth and local topographic height

Table 6 List and definitions of some metrics describing tsunami inland flooding, extracted from the IOC Tsunami Glossary (2019).

5.5.1.1 Theoretical background

At any point x between the shoreline ($x = 0$) and the maximum inundation ($x = x_R$, see Fig. 5.5.1), the flow mechanic energy above the ground, computed per unit weight (and then having dimension of a length), is given by the sum of kinetic and potential contributes, i.e.:

$$E = h + \frac{v^2}{g} \qquad (5.5.1)$$

Where h is the flow depth, v the velocity and g the gravitational acceleration. The energy grade line (marked by the dashed-red line in Fig. 20) accounts for the sum of E and the flow topographic gain, z. At the beginning of the profile, this coincides with the initial energy E_0, given simply by the sum of the kinetic ($K_0 = \frac{v_0^2}{g}$) and potential energy (h_0) contributions. Along the transect, the energy grade line decays due to friction effects induced by the interaction with the ground: this is denoted with the term D, accounting for dissipation effects of the flow while inundating the dry land. Then, energy conservation for each point of the profile leads to:

$$E + z + D = E_0 \quad (5.5.2)$$

Denoting the topography slope for each point as:

$$m = \frac{dz}{dx} \quad (5.5.3)$$

and the friction slope as:

$$S = \frac{dD}{dx} \quad (5.5.4)$$

We can differentiate Eq. 5.5.2 with respect to the distance along the transect and, introducing Eqs. 5.5.3 and 5.5.4, obtain:

$$\frac{dE}{dx} = -(m + S) \quad (5.5.5)$$

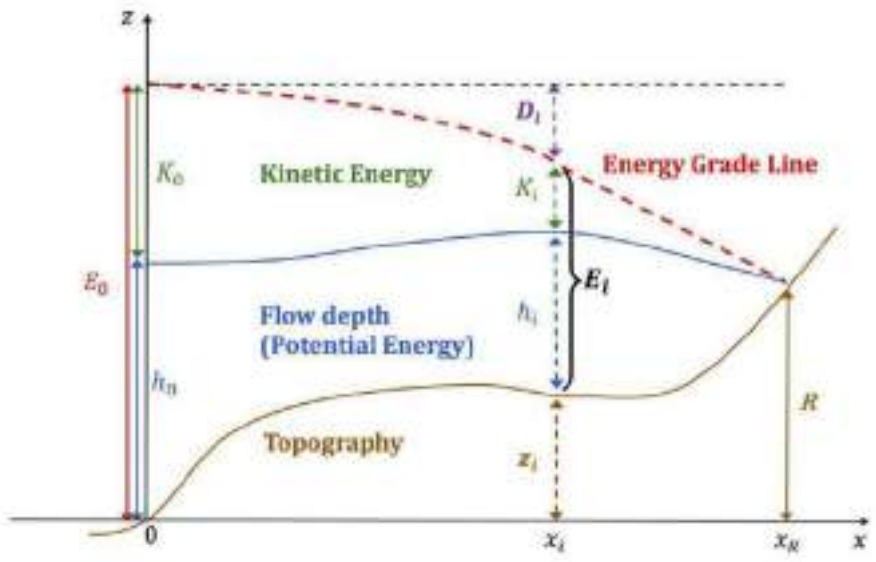

Figure 20 Sketch of the quantities involved in the energy balance along a flooded topographic profile.

The term S can be expressed through the Manning's equation:

$$S = n^2 v^2 h^{-\frac{4}{3}} \quad (5.5.6)$$

Where n is known as the roughness coefficient (or Manning's coefficient) and represents the dissipation affecting the flux while it inundates the ground. Eq. 5.5.5 written through Eq. 5.5.1 and 5.5.6 can't be solved, since it presents two unknowns, the flow depth h and its velocity v. To solve this indetermination, a further expression linking the two quantities is needed, i.e. the Froude number Fr relation, linking the flux velocity to the phase velocity, $\sqrt{gh}$:

$$v = Fr\sqrt{gh} \quad (5.5.7)$$

Which allow to rewrite Eq. 5.5.1 as:

$$E = h \cdot \left(1 + \frac{Fr^2}{2}\right) \quad (5.5.8)$$

And Eq. 5.5.6 as:

$$S = gn^2 Fr^2 h^{-\frac{1}{3}} \quad (5.5.9)$$

The unknowns are still two (h and Fr), but the last can be expressed through the law:

$$Fr = Fr_0 \cdot \left(1 - \frac{x}{x_R}\right)^{\frac{1}{2}} \quad (5.5.10)$$

Where Fr_0 is the value of the Froude number at the coast (usually considered unitary), and x_R is the maximum inundation, which should be then known a priori. These assumptions and considerations unravel the indetermination about Eq. 5.5.5, which depends only on the flow depth h, and can be then solved by means of numerical techniques, as shown in the following section.

5.5.1.2 Iterative procedure

As shown in the previous section, the ordinary differential equation 5.5.5 with the term specifications expressed by 5.5.8, 5.5.9 and 5.5.10 depends only on the flow depth h, and can be then solved numerically. There are many numerical schemes and techniques that can be implemented, the simplest of which is the Euler's method, a finite-difference scheme allowing to obtain the numerical solution v at the discrete time step i starting from its value at the previous numerical step, as:

$$v(i) = v(i-1) + \Delta x \cdot f(i-1) \quad (5.5.11)$$

Where f is the differential equation considered and Δx the discretization step. Eq. 5.5.5, then, can be solved through the following set of equations:

$$E(i) = E(i-1) - \Delta x \cdot [m(i) + S(i-1)] \quad (5.5.12)$$

with:

$$Fr(i-1) = Fr_0 \cdot \left[1 - \frac{x(i-1)}{x_R}\right]^{\frac{1}{2}} \quad (5.5.13)$$

$$h(i-1) = E(i-1) \cdot \left[1 + \frac{Fr(i-1)^2}{2}\right]^{-\frac{1}{2}} \quad (5.5.14)$$

$$S(i-1) = g \cdot n^2 \cdot Fr(i-1)^2 \cdot h(i-1)^{-\frac{1}{3}} \quad (5.5.15)$$

$$m(i) = \frac{z(i) - z(i-1)}{\Delta x} \quad (5.5.16)$$

At time step i all the quantities on the right of the equations are known, apart from x_R, representing the maximum inundation. In Kriebel et al. (2017) this was an input parameter, meaning that the flooding distance of the tsunami is an input data.

Here, since the aim is to calculate such distance as an output, a recursive procedure is implemented at each discrete iteration i, producing a preliminary assessment for x_R that is used as an input for further evaluations. The loop is stopped when such quantity converges. The initial value for comes from considerations on energy conservation. At the shoreline, the total energy is:

$$E_0 = h_0 \cdot \left(1 + \frac{{Fr_0}^2}{2}\right) \quad (5.5.17)$$

While, at the maximum inundation distance x_R, flow depth and velocities are zero and the energy is given by the topography, R , and the dissipative term. Invoking as initial assessment the no-friction condition, one gets simply:

$$E_R = R \qquad (5.5.18)$$

Since the energy must be conserved, we get from Eqs. 5.5.17 and 5.5.18 an estimation of the maximum expected runup for the tsunami amplitude at the coast, which can be considered an upper threshold, since it reached in non-dissipative conditions:

$$R = h_0 \cdot \left(1 + \frac{Fr_0^{\,2}}{2}\right) \qquad (5.5.19)$$

Accordingly, from this value it is possible to retrieve the inundation distance x_R along the topographic profile.

The initial condition E_0, necessary to start the numerical routine here described, is given by the expression 5.5.17.

5.5.2 Results

The numerical procedure previously described is implemented into a MatLab script, which requires as input the quantities already cited at the beginning of the Methods section. The roughness coefficient n (also known as Manning's coefficient, introduced in Eq. 5.5.6) must be provided. This parameter accounts for the energy dissipation of the flow during the flooding of the dry land, and depends on the nature of the inundated surface, which can facilitate or obstruct the inward flow. Table 7 reports some typical values of the roughness coefficient for different types of land use, both of natural and anthropic origin. Manning's coefficient units are usually omitted, but such parameter it's not dimensionless, being measured in $sm^{-\frac{1}{3}}$.

Land cover type	Reference value
Open Water	0.025
Developed, open space	0.035
Developed, low intensity	0.080
Developed, medium intensity	0.120
Developed, high intensity	0.150
Road	0.013
Railroad	0.033
Barren land (Rock/Sand/Clay)	0.030
Deciduous forest	0.100
Evergreen forest	0.150
Mixed forest	0.120
Grassland	0.040
Cultivated crops	0.050

Table 7 Reference values of the Manning's coefficient for different land cover types, retrieved from HEC-RAS2D manual (https://rashms.com/wp-content/uploads/2021/06/HEC-RAS-2D-Mannual-Mannings-n.pdf) and van der Sande et al. (2003).

The described procedure has been applied to two different cases of topographic profiles. The first one consists of a simplified morphology, with a mild constant gradient starting from the coast, followed by a 600 m long flat area and a steeper inland slope starting 800 m far from the shoreline (black line in Fig. 21). Three scenarios of initial tsunami amplitude have been considered: 2 m, 4 m and 8 m. For each of them, a no-dissipative condition is considered ($n = 0$), together with a low dissipation configuration ($n = 0.030$, corresponding to a sandy beach, for example). The tool has been run for each configuration, providing the flow depth (left column of plots in Fig. 21) and the velocity (right column of plots) profiles along the transect. As obvious, when

dissipation is neglected, the flow depth (in cyan) is higher; considering instead low dissipation produces some difference, visible especially in the $h_0 = 4\,m$ sketch (central low of plots), where runup and maximum inundation are respectively about 4 m and 450 m for the dissipative case (blue line), in contrast with 6 m and more than 800 m for the non-dissipative one. The difference is way smaller for the other two cases, mainly because the flux stops along the incline.

The same approach has been applied to a realistic topography, reported in Fig. 22, where a steep coastal slope is followed by a milder area and by a depression at a distance between 150 m and 200 m from the shoreline. While the values for h_0 are the same as the previous case, two different configurations of the roughness coefficients have been explored, reflecting two possible levels of anthropic coastal environment: $n = 0.035$ (developed, open space) and $n = 0.150$ (developed, high intensity). It is quite interesting to observe the different behavior of the flow depth profile in the two cases, especially for the $h_0 = 4\,m$ and $h_0 = 8\,m$ cases (middle and bottom row of plots in Fig. 22): lower dissipation values (cyan lines) produce much higher runups and maximum inundations (6 m – 80 m and 12 m - 200 m respectively for $h_0 = 4\,m$ and $h_0 = 8\,m$), while high roughness inhibits consistently the flooding, resulting into runups (3 m and 6 m) that are smaller than the respective amplitude at the coast. This configuration can be adopted, for example, for highly urbanized coasts, where huge buildings and structures can prevent the flux inundation even though they are not considered in the topographic profile.

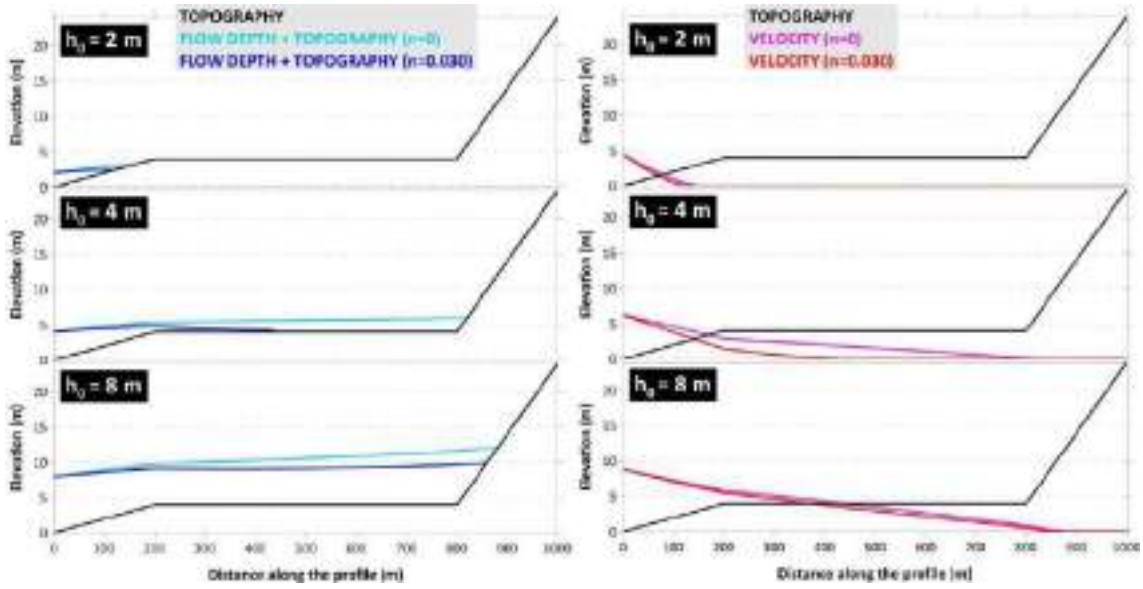

Figure 21 Examples of application of the tsunami flooding tool to a simplified topography (black line). Initial tsunami amplitudes of 2 m, 4 m and 8 m are considered; Manning's coefficient values of 0 (no dissipation) and 0.030 (barren land) have been selected. The respective flow depths are reported in cyan and blue (left column of plots); the respective flow velocities are in magenta and red (left column of plots).

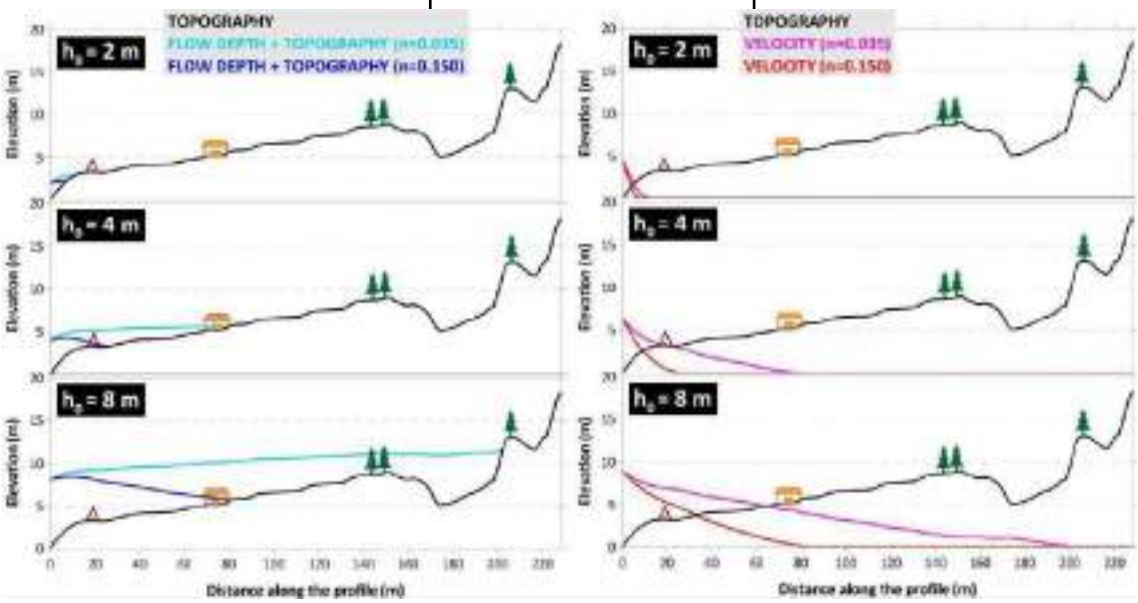

Figure 22 Examples of application of the tsunami flooding tool to a realistic topography (black line). Initial tsunami amplitudes of 2 m, 4 m and 8 m are considered; Manning's coefficient values of 0.035 (developed, open space) and 0.150 (developed, high intensity) have been selected. The respective flow depths are reported in cyan and blue (left column of plots); the respective flow velocities are in magenta and red (left column of plots).

5.5.2.1. Comparison with flooding from numerical simulations and observations

To validate the results obtained through the Energy Method application, a comparison between the flow depth and velocity retrieved with numerical simulation is presented in the following. The case study is a scenario of an earthquake-generated tsunami, which effects in the Siracusa Bay are simulated by means of the numerical code UBO-TSUFD, developed and maintained by the University of Bologna Tsunami Research Team (for details about the code see Tinti and Tonini, 2013). The results are shown in Fig. 23.

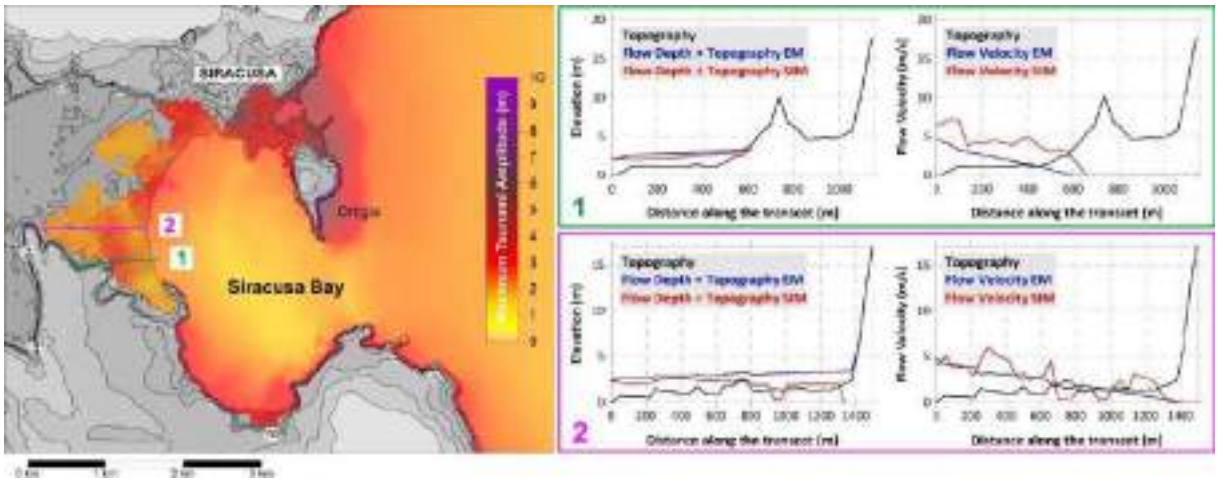

Figure 23 Left panel) Map of the Siracusa Bay and of the maximum tsunami amplitude on each node of the computational grid (yellow-red-purple scale). The green and magenta lines mark the topographic transects on which the comparison is performed. Right panels) Comparison between the flow depth and

the flow velocity obtained through the tool here presented (in blue) and the ones produced by the numerical simulations (in red). The black line marks the topographic profile of the two transects.

The two portrayed transects have different morphologies, reflecting into the tsunami penetration and runup: for profile 1 the initial tsunami amplitude is $h_0 = 2.1\ m$, and the maximum inundation results in 600 m, due to a topographic relief stopping the tsunami inland flooding (Figure 23, upper right panel). As concerns profile 2, a similar amplitude at the coast ($h_0 = 2.3\ m$) produces a much longer maximum inundation, almost 1400 m, due to the almost flat topography in that area (Fig. 23, lower right panel). The comparison between the flooding obtained through the Energy Method (in blue) and the one resulting from the numerical simulations (in red) is quite satisfying, especially for the flow depth along profile 1; in this case, the flow velocity is underestimated. Along profile 2, the tool produces an overestimation of the flow depth, probably since the tsunami flooding spreads over a large area, a feature that can't be captured by the 2D analysis carried out through the Energy Method; on the contrary, the flow velocities can be considered quite similar. In both cases, and in the numerical simulations as well, a non-dissipative configuration has been considered, i.e.

5.5.3 Novelty, Criticalities and Relevance/Potentiality of this tool

The impact of tsunami flooding on coastal buildings and infrastructures can be evaluated through numerical models, accounting for the water inundation with continuously growing accuracy and efficiency. However, there is also the need for fast assessment of the flooding process, especially in engineering applications needing conservative estimations of the tsunami flow depth or velocity. The tool here described implements the Energy Method approach, described in detail in Kriebel et al. (2017), into a recursive, numerical routine that improves such technique, originally requiring the maximum inundation as input as well: here, such quantity is provided in output, together with the flow depth and velocity profiles along a topographic transects.

The advantages of such approach are various: the numerical routine solves an ordinary differential equation through a finite-difference scheme, providing rapidly the output (typically in few seconds), in contrast with full tsunami numerical modelling requiring hours or tens of hours to be run. The method provides the outputs for each point of a topographic transect, allowing then to estimate quantities describing the flow impact on the structures object of the investigation, or also on population on the shoreline. Moreover, the points of maximum inundation can be used for hazard and risk assessment, through the individuation of potential flooded areas, contribute also to the definition of emergency plans, such as the case portrayed in Fig. 24, implementing this approach for the case of the Tavernola potential landslide-tsunami (Iseo Lake, northern Italy; Zaniboni et al., 2021). Starting from numerical simulations of the wave generated by the landslide, it is possible to assess the maximum tsunami amplitude on each point of the coastline. This information is used to provide the initial condition at a set of topographic transects (in blue), which the Energy Method is applied to. Connecting the points of maximum inundation obtained for each profile, it is possible to retrieve the maximum inundation line (in magenta), together with the lines of at least 1 m (orange) and 2 m (dark red) flow depth.

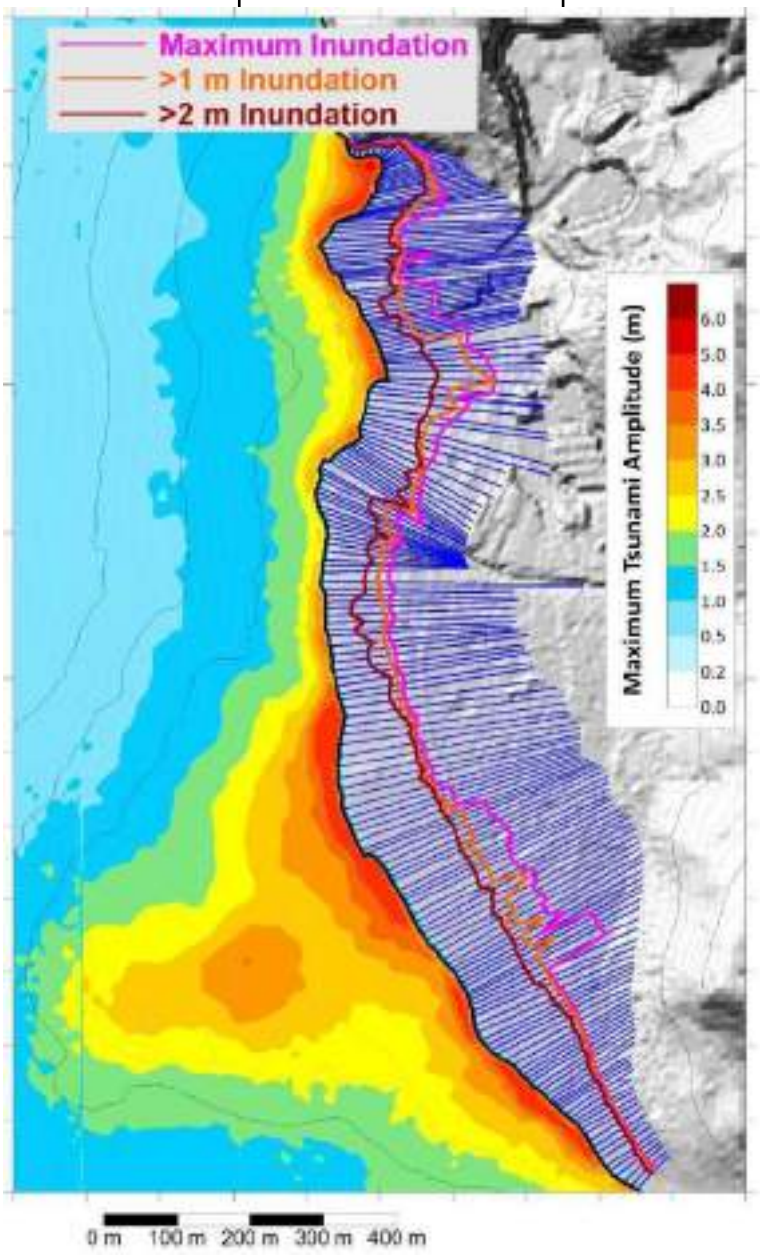

Figure 24 Estimation of inundated area from the potential landslide-tsunami of Tavernola, Iseo Lake (North Italy). The cyan-green-yellow-red scale marks the maximum tsunami amplitude over each node of the computational domain, obtained through numerical simulations. The blue lines indicate the topographic transects, where the Energy Method is applied. Connecting the points of maximum inundation, one can obtain the maximum inundation line (in magenta). Similarly, the 1 m and 2 m flow depth lines are retrieved (respectively in orange and dark red).

Like every simplified approach, also the Energy Method entails some drawbacks. The first and more obvious is that with a 2D approach some features of the tsunami flooding are lost, such as the wave lateral spreading when large areas are inundated, or, for peculiar morphologies, the opposite phenomenon, i.e. flow concentration or channeling (for example along rivers). Also, coastal hills or reliefs can be circumvented by the incoming flux, inundating also their back side that in the EM approach would be protected by the topography: effects of this type are lost, as well.

The method assumes that a tsunami is a constant flow entering from the coastal point, while it consists of a series of oscillations with period that can range from some to tens of minutes: for this reason, it generally provides an overestimation of the tsunami flooding, that in a tsunami hazard perspective is totally acceptable.

Furthermore, the topographic transect is usually retrieved from DEMs or other datasets that usually do not include building information, such as their elevation or dimensions, while in some cases they can act as physical barriers to tsunami inundation. This weakness can be partially tackled using high values for the Manning's coefficient, as shown for the second profile (Fig. 22), but the tool could also be applied to topographic transects integrating the sections of high buildings or structures located along the profile, if necessary.

A potential improvement of the tool can be the inclusion of a variable roughness coefficient along the transect now, the dissipation is constant along the profile and represented by a single value. A heterogeneous Manning's coefficient is perfectly reasonable (for example in a sandy beach with high hotels some hundreds of meters from the shoreline), and can be easily implemented in the numerical resolution, simply considering n as a vector containing a roughness value for each point of the topographic profile. This would require an accurate knowledge of the coastal setting, not always available, and more easily representable by a single coefficient.

13. 6. Third Chapter: From toolchains to the RETURNLAND Virtual Test Bed

The newly generated toolchain workflow for rapid marine landslides is designed to model hazard scenarios within the **RETURN Virtual Test Bed (VTB)**, a digital platform developed as part of **Task 2.4.1**. This platform leverages high-resolution digital elevation models (DEMs), both marine and terrestrial, with accuracies up to **5 cm** (in the terrestrial environment), derived from **Learning Examples (LEs)** that provide comprehensive geological data. These DEMs are integral for simulating, testing, and analyzing real-world processes related to submarine landslides. The table below reports input and output parameters used to generate the toolchain workflow and described in the previous chapters. The tools operate in sequence, with each output subsequently fed into the next, as indicated by the toolchain arrow on the right in the table below.

Factors	Tools	Input	Output	
Preconditioning	Canyon Retreat Susceptibility	1) Slope; 2) Uplift Rates; 3) GNSS horizontal rate; 4) GNSS vertical rate; 5) GNSS 2nd invariant; 6) InSAR vertical rate; 7) Canyon head - River mouth distance; 8) Canyon head - River mouth distance/ Canyon head - Coast Distance; 9) River mouth number in a 4km circular buffer; 10) Relief/Topographic Variance metrics; 11) Instrumental Earthquake number in a 4km circular buffer; 12) Synthetic Earthquake number in a 4km circular buffer;	Susceptibility classification	TOOLCHAIN
	Susceptibility analysis	Local scale -> Target: Landslide initiation Point (LIP) Preconditioning factors: 1) Slope; 2) Aspect; 3) Distance from river mouths; 4) Distance from faults; 5) Simplified lithological map	Susceptibility maps	
Preparatory	Factor of Safety in presence of Active Fluid Seepages	soil parameters related to preparatory factors and geotech. parameters	FOS critical threshold (under MS algorithm)	
Triggers	Landslide Tsunami propagation	- Morphological parameters of the landslide: 1) Volume 2) Barycentre depth 3) Average initial slope - Distance of coastal point(s) from the landslide barycentre	Maximum tsunami amplitude on the coastal point(s)	
	Landslide Tsunami Flooding	- topographic transect starting from the coastline (2D: distance, elevation) - tsunami amplitude at the coast	Flow depth and flood velocity along the transect	

Table 8 Summary of input and output parameters used to generate the toolchain workflow. The tools operate sequentially, with each output serving as the input for the subsequent tool, as indicated by the toolchain arrow on the right.

6.1 The Virtual Test Bed (VTB) RETURNLAND

The Virtual Test Bed (VTB) RETURNLAND has been designed as a functional demonstrator of a (multi)hazard tool chain capable of triggering *impact chains* on downstream urban VTBs. Its purpose is not to validate models, but rather to showcase how different components of the tool chain can be integrated into a coherent and operational workflow, enabling the representation of complex, interconnected scenarios involving geohazards and systemic impacts on urban and infrastructural environments.

As part of the RETURNLAND project, the marine sector includes a submerged portion of the virtual model that covers approximately 17,000 km², accounting for about 45% of the entire RETURNLAND domain. This area was selected due to its high relevance for the study of geohazards, particularly in zones characterized by

unstable slopes, submerged cliffs, and environments potentially prone to pore pressure buildup and liquefaction.

Within this context, we focused specifically on submarine landslides with rapid kinematics, as they can swiftly displace large volumes of the water column and potentially generate tsunamis within a short timeframe. Unfortunately, the limited number of representative examples has significantly constrained the development of comparable analyses for other types of submarine ground instabilities, such as slow-moving landslides, liquefaction-related failures, and landslides occurring along steep submarine cliffs.

The VTB was created by merging a series of Digital Elevation Models (DEMs) from various databases. The generation of this synthetic DEM involved several key steps. First, the reference systems of the individual DEMs were transformed to a common coordinate system (EPSG:32633 – WGS 84 / UTM zone 33N). Next, the DEMs were aligned using rigid transformations (translations and rotations), considering their elevation values and minimizing discrepancies between them. Once aligned, the DEMs were merged to form the final VTB.

For the marine portion, due to significant depth differences among the original DEMs, some localized areas were enhanced using contour lines to ensure better continuity between datasets. This entire workflow was carried out using various GIS software tools, including Global Mapper, ArcGIS, and QGIS.

The marine areas selected for inclusion, along with the main characteristics of the individual DEMs and their bathymetric data sources, are detailed below

- **Gulf of Palermo (Sicily)**: Submarine pockmarks in the escarpment area located a few km from the coastline. *Data provider: Valeria Lo Presti – Università di Palermo*
- **Open slope, Assi submarine landslide (Ionian Calabria):** Tsunamigenic submarine landslides. ***Data provider:*** *Silvia Ceramicola - OGS*
- **Fiumara Corace-Squillace canyon system (Ionian Calabria)**. Fiumara directly connected to a near coast submarine canyon head. ***Data provider****: Silvia Ceramicola - OGS*
- **Gioia Tauro (Tyrrhenian Calabria)**. Submarine canyons with near coast heads. ***Data provider****: Francesco Latino Chiocci - "La Sapienza" University of Rome*

The data (DEMs) provided is intended **solely for the generation of the VTB**; any other use requires prior authorization from the data owner. **If the data is published, proper attribution must be given, and the data author must be explicitly acknowledged.**

The seascape of the VTB has been selected to serve as a dynamic environment for modeling and assessing various hazard scenarios, simulating both local and regional-scale submarine landslide events. Specifically, it will facilitate the exploration of landslides occurring at **canyon heads**, where landslides tend to be more frequent and smaller in scale, as well as **open slopes**, which may produce larger, more catastrophic events with longer recurrence intervals. By incorporating the newly developed toolchain workflow, the VTB will enable the comprehensive simulation of preconditioning factors, preparatory processes, and triggers that initiate rapid submarine landslides.

The insights gained from these VTB scenarios are expected to play a critical role in advancing our understanding of submarine landslide dynamics. These results will be used to support the development of a **Proof of Concept (PoC)** for **rapid submarine landslides**, which will serve as a key validation tool for both **local hazard assessments** (focused on specific areas like canyon heads) and **regional hazard assessments** (focused on broader open slope environments). The PoC will help demonstrate the practical applicability of

the toolchain workflow in assessing real-world marine geohazard risks, providing valuable information for risk mitigation strategies and decision-making processes.

Ultimately, the VTB, powered by the validated toolchain, will allow researchers to test different mitigation strategies, evaluate hazard scenarios with unprecedented accuracy, and develop more effective risk management approaches for coastal areas and offshore infrastructures vulnerable to submarine landslides.

6.3 Final remarks and future perspective for geohazard assessment in coastal areas

As we advance in the understanding and assessing of marine geohazards, the integration of high-resolution data, reliable analytical tools, and interdisciplinary approaches becomes increasingly vital. The work carried out in the **RETURN within TASK 2.4.1** has contributed significantly to enhancing our ability to assess submarine landslides and their associated risks, particularly in coastal environments. The development of the first **susceptibility maps** for south Italy to analyse the influence of key landslide **predisposing factors**, and the creation of new reliable analytical tools for quantifying **preparatory factors** and **triggering mechanisms** have laid the groundwork for more precise risk assessments. These achievements mark a key step forward in our ability to assess the likelihood of submarine landslides and their potential impact on coastal populations and infrastructures.

Despite these remarkable advancements, several challenges remain. The dynamic nature of the marine environment, the complexity of underwater processes, and the difficulty in monitoring and predicting rapid, large-scale geohazard events all contribute to the uncertainty inherent in geohazard assessment. Furthermore, the Mediterranean Sea, with its highly active tectonic setting and numerous vulnerable assets, presents a particularly complex environment for geohazard risk mitigation. The proximity of coasts and narrow continental shelves in this region makes coastal areas even more vulnerable to events like submarine landslides that can generate tsunamis, often rendering traditional early warning systems ineffective.

Looking forward, the next phase of geohazard assessment must focus on improving our ability to continuously monitor marine environments. This will require a combination of **real-time data collection**, **advanced sensor networks**, and the further refinement of **analytical tools** able to account for the various triggers that lead to submarine landslides. The role of virtual platforms like **VTB (Virtual Test Bed)** in testing analytical tools and the development of a **PoC (Proof of Concept)** for marine landslides will be crucial for several reasons. These platforms allow for the testing and refinement of models in controlled, simulated environments that closely replicate real-world conditions, without the high costs and logistical challenges of full-scale implementation. VTB enables researchers to explore various scenarios, test different analytical methods, and assess the robustness of predictive models under a wide range of conditions, all while ensuring safety and minimizing risks. Several relevant types of submarine ground instabilities—such as **liquefaction in nearshore or insular areas**, **submerged sinkholes**, and **sediment subsidence on continental shelves**—have not yet been addressed within the current (multi)hazard scenarios of the submerged sector, although they are considered in the onshore domain. These processes, while well-recognized on land, remain underrepresented offshore despite their potential relevance in densely used or sensitive coastal and insular zones.

The **PoC** development, on the other hand, allows for practical demonstrations of these models, confirming their viability and performance in real-world settings. It is a crucial step before widespread adoption, as it validates the theoretical models and analytical tools developed during the research phase. By testing these models and tools in actual marine environments, PoC will help to identify gaps in knowledge, refine toolchain workflow, and will help in providing efficient risk mitigation strategies.

As the field of geohazard, especially regarding submarine landslides, continues to evolve, these virtual platforms will be indispensable in accelerating innovation and refining mitigation strategies for coastal and nearshore risks.

In the future, we intend to **adapt and transfer the tools developed for onshore hazard assessment** to nearshore marine environments, with the goal of extending their applicability to these neglected processes. This would support the treatment of both **multiple hazards** (simultaneous but not necessarily interacting) and **multi-hazard scenarios** (cascading or interacting events), improving the comprehensiveness of hazard modeling in the submerged domain. A critical assessment of the **transferability and representability** of multiple (non-interacting) hazard scenarios in the offshore context should also be considered, particularly with regard to their integration into broader coastal risk frameworks.

Moreover, a more integrated approach to **multi-hazard risk assessment** is essential, as submarine landslides can trigger or amplify other geohazards such as earthquakes and tsunamis. Expanding the newly developed toolchain to incorporate these interrelated processes will improve our understanding of their combined impacts on coastal communities and infrastructure.

Future work should also focus on translating these advancements into practical guidelines for **coastal resilience** and **infrastructure protection**. This includes developing better **risk mitigation strategies**, **early warning systems**, and **adaptation measures** to safeguard vulnerable coastal populations. Additionally, with the increasing importance of sectors such as energy production in the context of the energy transition, geohazard risk assessment will become even more critical in ensuring the safety of these vital sectors.

In conclusion, while significant progress has been made in the field of marine geohazard assessment, much work remains to be done. By continuing to refine our methodologies, enhance monitoring capabilities, and develop integrated risk assessment frameworks, we can better understand, quantify, and mitigate the risks posed by submarine landslides and other marine geohazards. This will ultimately contribute to more resilient coastal communities and infrastructures.

14. 7. References

- Avdievitch, N.N., Coe, J.A., 2022. Submarine Landslide Susceptibility Mapping in Recently Deglaciated Terrain, Glacier Bay, Alaska. Frontiers in Earth Science, 10.
- Catalano, R., Di Maio, D., Sulli, A., Analfino, A. (2013). Carta Geologica d'Italia alla scala 1:50.000 del Foglio 599 "Patti (settore marino)". Progetto CARG. Roma: ISPRA - Servizio Geologico d'Italia.
- Ceramicola S., Tinti S., Zaniboni F., Praeg D., Planinsek P., Pagnoni G., Forlin E. (2014). Reconstruction and tsunami modeling of a submarine landslide on the Ionian margin of Calabria (Mediterranean Sea), K. Sassa, P. Canuti, Y. Yin (eds.), Landslide Science for a Safer Geoenvironment, Vol. 3, pp. 557-562, © Springer International Publishing Switzerland, doi: 10.1007/978-3-319-04996-0_85.
- Ceramicola, S., A. Cova, E. Forlin, N. Markezic, G. Mangano, D. Civile, M. Zecchin, F. Fanucci, E. Colizza, C. Corselli, D. Morelli, A. Savini, A. Caburlotto, O. Candoni, M. Coste, D. Cotterle, S. Critelli, A. Cuppari, M. Deponte, R. Dominici, L. Facchin, E. Gordini, M. Locatelli, F. Muto, D. Praeg, R. Romeo, C. Tessarolo (2024) Geohazard Features of the Ionian Calabrian margin. Journal of Maps 20 (1), 2349785, https://doi.org/10.1080/17445647.2024.2349785.
- Ceramicola, S., M. R. Senatore, A. Cova, A. Meo, E. Forlin, S. Critelli, N. Markezic, M. Zecchin, D. Civile, A. Bosman, O. Candoni, D. Casalbore, M. Coste, D. Cotterle, M. Deponte, R. Dominici, L. Facchin, E. Gordini, E. Morelli, F. Muto, D. Praeg, R. Romeo, F. L. Chiocci (2024) Geohazard Features of the Gulf of Taranto. Journal of Maps 20 (1), 2431073, https://doi.org/10.1080/17445647.2024.2431073.
- Chiocci, F.L., Ridente, D., 2011. Regional-scale seafloor mapping and geohazard assessment. The experience from the Italian project MaGIC (Marine Geohazards along the Italian Coasts). Mar Geophys Res 32, 13–23. https://doi.org/10.1007/s11001-011-9120-6
- Crosetto, M., Solari, L., Balasis-Levinsen, J., Bateson, L., Casagli, N., Frei, M., Oyen, A., Moldestad, D.A., Mróz, M., 2021. DEFORMATION MONITORING AT EUROPEAN SCALE: THE COPERNICUS GROUND MOTION SERVICE. The International Archives of the Photogrammetry, Remote Sensing and Spatial Information Sciences XLIII-B3-2021, 141–146. https://doi.org/10.5194/isprs-archives-XLIII-B3-2021-141-2021
- D'Ascola, F., Cassese, M.L., Lugeri, N., Pesarino, V., Salmeri, A., 2022. The ISPRA geodatabase for monitoring and analysis of the state of the italian coasts: an example of its application to the Rocchette - Castiglione della Pescaia coast line, in: Bonora, L., Carboni, D., De Vincenzi, M., Matteucci, G. (Eds.), Ninth International Symposium "Monitoring of Mediterranean Coastal Areas: Problems and Measurement Techniques." Firenze University Press. https://doi.org/10.36253/979-12-215-0030-1.03
- Ferranti, L., Antonioli, F., Mauz, B., Amorosi, A., Dai Pra, G., Mastronuzzi, G., Monaco, C., Orrù, P., Pappalardo, M., Radtke, U., Renda, P., Romano, P., Sansò, P., Verrubbi, V., 2006. Markers of the last interglacial sea-level high stand along the coast of Italy: Tectonic implications. Quaternary International, Quaternary sea-level changes: contributions from the 32nd IGC 145–146, 30–54. https://doi.org/10.1016/j.quaint.2005.07.009
- Gallotti G., Zaniboni F., Arcangeli D., Angeli C., Armigliato A., Cocchi L., Muccini F., Zanetti M., Tinti S., Ventura G. (2023). The tsunamigenic potential of landslide-generated tsunamis on the Vavilov seamount. Journal of Volcanology and Geothermal Research, 434, 107745. https://doi.org/10.1016/j.jvolgeores.2023.107745.

- Gasperini L., Zaniboni F., Armigliato A., Tinti S., Pagnoni G., Özeren M. S., Ligi M., Natali F., Polonia A. (2022). Tsunami potential source in the eastern Sea of Marmara (NW Turkey), along the North Anatolian Fault system. Landslides, 19:2295–2310. DOI 10.1007/s10346-022-01929-0.
- Geoportale RNDT [WWW Document], n.d. URL https://geodati.gov.it/resource/id/ispra_rm:01Idro250N_DT (accessed 4.11.25).
- Harbitz, C.B., Løvholt, F., Bungum, H., 2013. Submarine landslide tsunamis: how extreme and how likely? Natural Hazards, 72(3), 1341-1374.
- Innocenti, C., Battaglini, L., D'Angelo, S., Fiorentino, A., 2020. Submarine landslides: mapping the susceptibility in European seas. Quarterly Journal of Engineering Geology and Hydrogeology, 54(1).
- Intergovernmental Oceanographic Commission (2019), Tsunami Glossary. Fourth Edition. Paris, UNESCO. IOC Technical Series, 85. (English, French, Spanish, Arabic, Chinese) (IOC/2008/TS/85 rev.4).
- Kriebel D. L., Lynett P. J., Cox D. T., Petroff C. M., Robertson I. N., Chock G. Y. (2017). Energy method for approximating overland tsunami flows. Journal of Waterway, Port, Coastal, and Ocean Engineering, 143(5), 04017014. https://doi.org/10.1061/(ASCE)WW.1943-5460.0000393.
- Kuhlmann, J., Asioli, A., Trincardi, F., Klügel, A., and Huhn, K. (2017). Landslide frequency and failure mechanisms at NE Gela Basin (Strait of Sicily). J. Geophys. Res.: Earth Surf. 122, 2223–2243. doi:10.1002/2017JF004251.
- Løvholt F., Pedersen G., Harbitz C.B., Glimsdal S. and Kim J. (2015). On the characteristics of landslide tsunamis. Phil. Trans. R. Soc. A 373: 20140376. DOI: 10.1098/rsta.2014.0376.
- Løvholt, F., S Glimsdal, CB Harbitz (2025) Tsunami hazard from subaerial landslides Probabilistic Tsunami Hazard and Risk Analysis, Elsevier, 289-301, https://doi.org/10.1016/B978-0-443-18987-6.00010-5
- METIQ working group (2023). Quaternary map of Italy, scale 1:500.000, 5 sheet edited by ISPRA, Draft version edited for INQUA Congress, Roma.
- Nian, T.-k., Guo, X.-s., Zheng, D.-f., Xiu, Z.-x., Jiang, Z.-b., 2019. Susceptibility assessment of regional submarine landslides triggered by seismic actions. Applied Ocean Research, 93.
- Noda A., TuZino T., Joshima M. and Goto S. (2013). Mass transport-dominated sedimentation in a foreland basin, the Hidaka Trough, northern Japan. *Geochemistry Geophysics Geosystems*, 14, 2638–2660, doi:10.1002/ggge.20169
- Palano, M., Piromallo, C., Chiarabba, C., 2017. Surface imprint of toroidal flow at retreating slab edges: The first geodetic evidence in the Calabrian subduction system. Geophysical Research Letters 44, 845–853. https://doi.org/10.1002/2016GL071452
- Rahiman T. I. and Pettinga J. R. (2006). The offshore morpho-structure and tsunami sources of the Viti Levu Seismic Zone, southeast Viti Levu, Fiji. Marine Geology, 232(3-4), 203-225. https://doi.org/10.1016/j.margeo.2006.07.007.
- Rovida, A., Locati, M., Camassi, R., Lolli, B., Gasperini, P., 2020. The Italian earthquake catalogue CPTI15. Bull Earthquake Eng 18, 2953–2984. https://doi.org/10.1007/s10518-020-00818-y

- Sultan, N., Cochonat, P., Canals, M., Cattaneo, A., Dennielou, B., Haflidason, H., Laberg, J.S., Long, D., Mienert, J., Trincardi, F., Urgeles, R., Vorren, T.o. and Wilson, C. (2004) *Triggering mechanisms of slope instability processes and sediment failures on continental margins: a geotechnical approach.* Marine Geology, 213(1-4), 291-321. DOI: http://dx.doi.org/10.1016/j.margeo.2004.10.011
- Tinti S. and Tonini R. (2013) The UBO-TSUFD tsunami inundation model: validation and application to a tsunami case study focused on the city of Catania, Italy, Nat. Hazards Earth Syst. Sci., 13, 1795–1816, www.nat-hazards-earth-syst-sci.net/13/1795/2013/, doi: 10.5194/nhess-13-1795-2013.
- Van der Sande C. J., De Jong S. M., De Roo A. P. J. (2003). A segmentation and classification approach of IKONOS-2 imagery for land cover mapping to assist flood risk and flood damage assessment. International Journal of applied earth observation and geoinformation, 4(3), 217-229. https://doi.org/10.1016/S0303-2434(03)00003-5.
- Watts P., Grilli S. T., Tappin D. R. and Fryer G. J. (2005). Tsunami generation by submarine mass failure. I: predictive equations and case studies. J.Waterway, Port, Coastal, Ocean Eng. 131(6): 298–310. DOI: 10.1061/(ASCE)0733-950X(2005)131:6(298).
- Yavari-Ramshe S. and Ataie-Ashtiani B. (2016). Numerical modeling of subaerial and submarine landslide-generated tsunami waves—recent advances and future challenges. Landslides (2016) 13:1325–1368. DOI: 10.1007/s10346-016-0734-2.
- Zaniboni F., Armigliato A., Pagnoni G., and Tinti S. (2014). Continental margins as a source of tsunami hazard: the 1977 Gioia Tauro (Italy) landslide-tsunami investigated through numerical modelling. Mar. Geol. 357 (2014), 210–217. doi:10.1016/j.margeo.2014.08.011.
- Zaniboni F., Armigliato A., Tinti S., Angeli C., Gallotti G., Zanetti M. (2021), Studio numerico del potenziale tsunami generato nel Lago d'Iseo dalla frana del Monte Saresano. Report commissioned by Autorità di Bacino Lacuale dei Laghi d'Iseo, Endine e Moro, Regione Lombardia (in Italian, available under request).
- Zaniboni F., Pagnoni G., Gallotti G., Tinti S., Armigliato A. (2024). Landslide-tsunamis along the flanks of Mount Epomeo, Ischia: propagation patterns and coastal hazard for the Campania Coasts, Italy. From: Marotta E., D'Auria L., Zaniboni F. and Nave R. (eds) Volcanic Island: from Hazard Assessment to Risk Mitigation. Geological Society, London, Special Publications, 519. https://doi.org/10.1144/SP519-2020-128.
- Zaniboni F., Pagnoni G., Paparo M.A., Gauchery T., Rovere M., Argnani A., Armigliato A. and Tinti S. (2021). Tsunamis From Submarine Collapses Along the Eastern Slope of the Gela Basin (Strait of Sicily). Front. Earth Sci. 8:602171. doi: 10.3389/feart.2020.602171.
- Zengaffinen-Morris T., Urgeles R., Løvholt F. (2022). On the inference of tsunami uncertainties from landslide run-out observations. Journal of Geophysical Research: Oceans, 127, e2021JC018033. https://doi.org/10.1029/2021JC018033.